THE ASTROPHYSICAL JOURNAL, 314:551–571, 1987 March 15

THE PLANETARY NEBULA NGC 3918[1]

R. E. S. CLEGG
Department of Physics and Astronomy, University College London
J. P. HARRINGTON
Astronomy Program, University of Maryland
M. J. BARLOW
Department of Physics and Astronomy, University College London
AND
J. R. WALSH
Anglo-Australian Observatory
Received 1986 February 13; accepted 1986 September 5

ABSTRACT

A detailed study of the planetary nebula NGC 3918, based on UV, optical, and radio observations, is presented. High- and low-resolution *IUE* and optical spectra are used to measure line fluxes. The electron temperature is obtained from eight sets of line ratios, and diagnostics for electron temperature show that the C II λ4267 line shows no significant anomaly in this object. Several carbon and nitrogen recombination lines are analyzed, and their use in determining C and N abundances is critically discussed. The central star has a predicted V-magnitude of 14.6, and a luminosity of 6900 $L_\odot$ for a distance of 1.5 kpc. A contour map of the nebula in Hβ light is given.

Velocity profiles of [O II] optical lines show that O^+ ions are mostly located at the front and rear of the nebula. A composite, biconical, model is constructed which consists of optically thick cones at the front and rear, with a low-density "equatorial" region which is optically thin, even in the He II continuum. Correction of the stellar He II Zanstra temperature, $T_Z = 117{,}000$ K, for this effect then enables us to use a non–LTE model atmosphere having $T_{\rm eff} = 140{,}000$ K. The nebular expansion age is in reasonable agreement with the age of the nucleus (since ejection of the nebula) found from evolutionary tracks: both are $\sim$3000 yr.

Silicon, magnesium, and iron are depleted by factors of 4, 3, and 100 respectively. It is shown that the Mg II λ2800 lines are affected by interstellar absorption in this and many other planetaries and thus often cannot be used for abundance determinations. About 60% of the stellar ionizing photons escape from the nebula, and the implications of such a "leaky" model for the ionization of the interstellar medium and Galactic halo are considered.

Subject headings: nebulae: abundances — nebulae: individual — nebulae: planetary — ultraviolet: spectra

I. INTRODUCTION

Planetary nebulae (PNs) represent the last stages of evolution for most stars in the Galaxy. Modeling these objects is of importance for the study of the properties of the central stars, the nebular abundances (especially for elements for which only a few ionization stages are seen), and for the study of physical processes occurring in dusty, ionized plasmas of low density. The analysis of gaseous nebulae rests on the results of the theory of atomic physics, and the interaction between these two subjects is rather important. In the present paper, for example, the processes of photoionization, radiative and dielectronic recombination, collisional excitation, and charge exchange are considered. A previous example of modeling PNs in detail was outlined by Harrington *et al.* (1982, hereafter HSAL), who analyzed NGC 7662.

In this paper we use and extend the methods of HSAL to make a highly detailed analysis of the bright southern planetary NGC 3918. It is of high excitation and has a high surface brightness such that the central star is not seen. It was selected because it shows rough circular symmetry in the sky with a less patchy appearance than that of NGC 7662, and because it shows spectral lines excited by dielectronic recombination (such as C III λ2297) and by charge transfer (such as O III λ5592). Useful information on the nebula can be obtained right across the electromagnetic spectrum; we used data extending from 1200 Å to 6 cm in wavelength in this work. The main sets of data used here are threefold: spectroscopic data (line fluxes), images (projected maps on the sky in Hβ and [O III] light), and two-dimensional velocity-position data which reveal something of the three-dimensional structure of the object.

Models of NGC 3918 have previously been given by Torres-Peimbert, Pena, and Daltabuit (1981), while an abundance analysis was made by Torres-Peimbert and Peimbert (1977, hereafter TPP). In our work we have drawn on the data sets of TPP and of Kohoutek and Martin (1981, hereafter KM) as well as on a large amount of new data, which are described in § II. Subsequent sections present an empirical analysis, information on the central star, and a photoionization model.

This is the main paper in a series concerning NGC 3918. A preliminary description of the work was given by Clegg, Harrington, and Barlow (1984), while applications of the nebular model to charge transfer and to dust processes were given by Clegg and Walsh (1985) and Harrington, Clegg, and Monk (1984) respectively. Separate publications will describe in more

[1] Based on observations obtained at VILSPA with the *IUE* satellite, which is operated jointly by NASA, ESA, and the UK SERC.

TABLE 1

IUE SPECTRA USED

Image Number	Date	Exposure (minutes)	Position Angle	Resolution
SWP 1906	1978 Jul 4	7	10°	Low
SWP 3191	1978 Nov 12	20	138	Low
SWP 3192	1978 Nov 12	10	138	Low
SWP 18028	1982 Sep 19	3	0	Low
SWP 18029	1982 Sep 19	50	0	Low
SWP 3215	1978 Nov 12	120	138	High
SWP 18030	1982 Sep 19	15	0	High
SWP 19888	1983 May 3	195	310	High
LWR 2809	1978 Nov 27	6	156	Low
LWR 1767	1978 Jul 3	12	9	Low
LWR 2753	1978 Nov 23	20	151	Low
LWR 8732	1980 Sep 6	35	60	Low
LWR 11432	1981 Aug 30	100	54	Low
LWR 14213	1982 Sep 19	55	0	Low
LWR 14215	1982 Sep 19	36	0	High
LWR 14222	1982 Sep 20	25	0	High
LWP 4096	1983 May 3	4.5	310	Low
LWP 2407	1983 Dec 14	180	173	High

detail work on modeling dust in NGC 3918 and on the velocity field.

In this paper continuum and line fluxes have been dereddened with the function $f(\lambda)$ from Seaton (1979). We use the notation $F(\lambda)$ and $I(\lambda)$ for observed and dereddened fluxes respectively.

II. OBSERVATIONS

a) IUE Data

Eight low- and five high-resolution spectra were obtained with the *IUE* satellite. Details of the exposures obtained by us, and of some images obtained from the *IUE* data center, are given in Table 1. All our *IUE* observations were made through the large aperture (LAP), which we show later covers 80% of the nebular Hβ emission. Although the nebula is extended, with a diameter of 17″ at 10% of central intensity, we were able to set directly and guide on the object during the exposures. This was presumably due to the smoothness and circular symmetry of NGC 3918, and it contrasts with the difficulties of guiding on NGC 7662 described by HSAL. The guiding accuracy was checked during some exposures by monitoring FES counts and by measuring offsets to nearby guide stars.

The variety of exposure times listed in Table 1 ensured that both weak and strong line fluxes and continuum levels could be measured from well-exposed (DN $\approx$ 120–200) spectra. The absolute fluxes, measured off the low-resolution spectra using extraction programmes written by Drs. J. Giddings and S. Adams at University College, are listed in Table 2 for the short-wavelength region and in Table 3 for the long wavelengths. Allowance was made for the fact that the extended nebula almost completely filled the *IUE* LAP.

High-resolution spectra were generally only used for the measurement of flux ratios of nearby lines, especially those used as density diagnostics, and to separate the contributions of lines blended at low resolution, such as Si IV and O IV] near 1401 Å and C II and [O III] near 2321 Å. An example of this is shown in Figure 1, where the components of the Si IV and O IV] multiplets, extracted from the image SWP 19888, are displayed. The ratio of O IV] lines 1401/1404 Å is a density diagnostic (see § III*b*). We also used the measurements of Pena and Torres-Peimbert (1985) for the relative fluxes of C III λ2297 and He II λ2307 in the image LWP 2407. That spectrum was also used to examine the Mg II lines near 2800 Å. Absolute fluxes from low-resolution spectra were always preferred if available because of uncertainties in the high-resolution calibrations and in echelle ripple corrections.

The doublet ratios for the components of the resonance lines of N V and C IV were measured off the high-dispersion spectra SWP 19888 and SWP 18030 respectively, in which the lines are well exposed. The ratios are R(N V λ1238/λ1240) = 1.6 $\pm$ 0.2 and R(C IV λ1548/λ1550) = 1.8 $\pm$ 0.2. Pena and Torres-Peimbert (1983) obtained values of 1.2 $\pm$ 0.1 and 1.9 $\pm$ 0.2 respectively for these ratios. More recently, Pena and Torres-Peimbert (1985) measured R as a function of image exposure time T in seven SWP spectra: R(N V) increased from 1.3 to 2.1 as T rose from 60 to 150 minutes, while R(C IV) varied between 1.7 and 2.1 for values of T between 15 and 30 minutes. These values are probably consistent with the theoretical ratio of 2.0 when allowance is made for uncertainties in the *IUE* intensity transfer function and echelle ripple corrections.

b) Optical Spectroscopy

Four sets of flux measurements from optical spectra, obtained at the 3.9 m Anglo-Australian Telescope (AAT) and

TABLE 2

OBSERVED FLUXES (10^{-12} ergs cm^{-2} s^{-1}) IN SWP LAP SPECTRA

λ (Å)	IDENTIFICATION	SWP[a]				
		18028 (3)	1906 (7)	3192 (10)	3191 (20)	18029 (50)
1176.....	C III	...	...	1.3	2.8	2.2
1240.....	N V	...	6.3	7.0	6.7	6.7
1342.....	O IV	...	...	...	...	0.4:
1401.....	O IV] + Si IV	10.6	11.0	9.1	9.8	10.8
1486.....	N IV]	...	11.9	11.3	9.4	11.6
1550.....	C IV	117	S	S	S	S
1576.....	[Ne V] + C III	...	...	...	1.1	1.3
1602.....	[Ne IV]	...	...	...	1.5	1.5
1641.....	He II	70	S	S	S	S
1664.....	O III]	...	6.7	8.0	8.4	S
1751.....	N III]	7.0	7.3	7.5	6.7	S
1908.....	C III]	113	S	S	S	S

[a] Parentheses enclose exposure times; S denotes saturated lines.

TABLE 3

OBSERVED FLUXES (10^{-12} ergs cm^{-2} s^{-1}) IN LWP AND LWR LAP SPECTRA[a]

λ (Å)	IDENTIFICATION	LWP 4096 (4.5)	LWR[b] 2809 (6)	1767 (12)	2753 (20)	8732 (35)	14213 (55)
1908.....	C III]	...	124	121	S	S	S
2300.....	C III + He II	...	...	...	...	1.2	1.3
2323.....	C II] + [O III]	12.3	9.4	10.0	9.0	8.6	S
2386.....	He II	...	...	1.1	0.98	0.90	0.82
2423.....	[Ne IV]	30	32	S	S	S	S
2470.....	[O II]	...	...	2.6	2.5	2.3	S
2512.....	He II	...	...	1.6	1.8	2.1	S
2733.....	He II	3.5	4.5	S	S	S	S
2783.....	Mg V]	1.6	...	2.1	1.8	S	S
2837.....	O III	...	4.7	4.2	3.9	S	S
3025.....	O III	...	3.9:	2.8	1.8	2.3	2.3
3047.....	O III	...	...	6.7	5.4	6.8	...
3133.....	O III	39	37	40	S	S	S
3187.....	He I	2.1	...	...	...	...	...
3204.....	He II	9.0	...	9.9	7.6	9.5	7.8

[a] Parentheses enclose exposure times.
[b] S denotes saturated lines.

the 1.9 m telescope of the South African Astronomical Observatory (SAAO), have been used. They consist of high-resolution spectra in the blue region, medium-resolution spectra taken at nine positions in the nebula, high-resolution spectra in the 5460–6080 Å region, and a low-resolution CCD spectrum extending from 5400 to 10,000 Å. We also drew on the published optical data of TPP and KM in our analysis. Typical errors in optical line fluxes are 30% for the weakest lines listed and 10% for the strong lines.

i) *High-Resolution Blue Spectra*

These were recorded at the AAT with an image photon counting system (IPCS) with the 25 cm camera and the RGO spectrograph, on 1981 July 22. The slit was oriented east-west, and the seeing was ~2″. Table 4 lists the spectra obtained; different neutral density filters were used to obtain unsaturated exposures of weak and strong lines. Flux calibration was made via the standard star W485A (Oke 1984). The wavelength range recorded was from 4240 to 4725 Å at a resolution of 0.7 Å in second order; a BG 38 filter was used to cut out first grating order. The spectra are two-dimensional: relative fluxes along the slit were obtained at positions (pixels) separated by 2″.2, and in the strongest line (Hγ 4340 Å) emission was detected over 20 pixels.

To obtain line fluxes relative to Hβ, we compared measurements with the Hγ line, whose strength relative to Hβ was taken from Brocklehurst (1971). The total fluxes (summed over all spatial positions) were compared for lines of interest in the

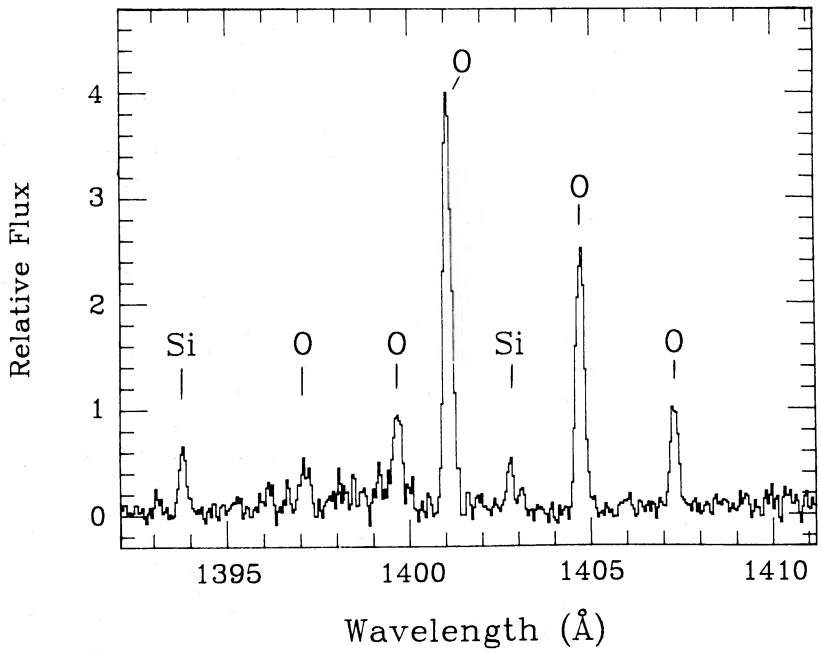

FIG. 1.—Part of the *IUE* high-resolution image SWP 19888, showing components of the Si IV ^2S–^2P and O IV $^2P^o$–^4P transisitions, as marked. The O IV ratio λ1401/λ1404 is a density diagnostic for $N_e < 10^4$ cm^{-3}.

TABLE 4

JOURNAL OF AAT HIGH-RESOLUTION SPECTROSCOPY

Run Number[a]	Exposure (s)	Slit Width		Neutral Density Filter
		Microns	Arcseconds	
8.....	400	1000	6.″7	0.7
9.....	150	1000	6.7	1.6
11.....	1300	230	1.5	...
13.....	50	230	1.5	1.0
14.....	150	230	1.5	1.3

[a] IPCS sequence number for spectrum taken.

five spectra, and a careful assessment made of the saturation in strong lines (the IPCS maximum count rate for emision lines is ~3 Hz). Unsaturated lines were then measured off the appropriate spectrum; it was thus assumed that the telescope guiding was accurate and that the position of the slit across the nebula was constant with time. Dereddened total fluxes in the summed spectra are listed in Table 5; they are taken from runs[2] 11 and 14, with slit width 1.″5 (see Table 4), and are taken to be representative of the whole object (wide- and narrow-slit spectra gave similar relative intensities).

[2] Run numbers are the IPCS image sequence numbers recorded in the AAT observing logs.

TABLE 5

AAT NARROW-SLIT FLUXES

λ (Å)	Identification	$f(\lambda)$	$I(\lambda)$
4267.1.....	C II	0.141	0.43
4275.8.....	O II	0.139	0.033
4303.8.....	O II	0.133	0.054
4340.2.....	Hγ	0.124	47.2
4363.2.....	[O III]	0.119	20.2
4376.5.....	...	0.116	0.03:
4379.2.....	N III	0.115	0.16
4387.8.....	He I	0.113	0.33
4391.6.....	...	0.112	0.013:
4400.9.....	...	0.110	0.11
4414.7.....	O II	0.107	0.035
4437.5.....	He I	0.102	0.035
4443.7.....	Ne II	0.100	0.29
4448.0.....	O II	0.099	0.019
4452.7.....	...	0.098	0.049
4471.5.....	He I	0.094	2.85
4510.9.....	N III	0.084	0.080
4514.9.....	N III	0.083	0.013
4523.6.....	N III	0.081	0.019
4534.5.....	N III	0.079	0.029
4541.7.....	He II	0.077	1.42
4562.4.....	Mg I]	0.072	0.066
4571.0.....	Mg I]	0.070	0.34
4590.9.....	O II	0.065	0.026
4606.4.....	N IV	0.061	0.065
4625.3.....	[Ar V]	0.057	0.051
4631.7.....	O IV	0.055	0.15
4633.9.....	N III	0.055	1.58
4640.6.....	N III	0.053	3.64
4647.1.....	C III	0.052	0.22
4650.3.....	C III + O II	0.051	0.42
4658.2.....	C IV	0.049	0.42
4661.9.....	O II	0.048	0.035
4685.0.....	He II	0.042	49.9
4710.5.....	[Ar IV]	0.036	5.6
4712.6.....	He I	0.036	0.62

The variation of line intensities across the nebula is of importance in determining the ionization structure. For example, the edge of the He^+ Strömgren sphere in the planetary NGC 7662 is clearly visible in the image in He II λ4686 light (Kupferman 1983), and the edge appears also in the model of HSAL. We have measured fluxes of selected lines at 20 positions along east-west slits across NGC 3918: the results for six lines are given in Table 6. The dereddened fluxes given there are obtained via the Hγ flux and using $c = 0.43$. The fluxes listed for Hγ and He II λ4686 in Table 6 show that these lines were detected out to radii of 21″ from the nebular center, with intensities only 3×10^{-4} the central intensity. This weak emission extends well beyond the limit of the Hβ contour map described in § IIc, where the plate limit is reached at a radius of 13″ in the east-west direction. Moreover, the ratio of He II to Hγ does not vary much across the object, and we do not see evidence for the detection of the edge of the He^+ Strömgren sphere. An explanation for the faint outer "halo" and the roughly constant 4686 Å flux is given in § Vc.

Of particular interest in these spectra are permitted recombination lines of C II, C III, and C IV. In a series of papers, Barker (e.g., 1984, 1985) presented evidence that the important C II *3d–4f* line at 4267 Å is anomalously strong, compared to C III λ1908, near the centers of some PNs. We examined the profile of 4267 Å carefully to check for any blend with another line. In our spectra the line is well fitted by a Gaussian with center 4267.2 Å and FWHM 1.3 Å, while for Hγ these parameters are 4340.2 Å and 1.6 Å (the widths are determined by nebular expansion plus the instrumental profile). The C II line is a doublet with components at 4267.02 Å and 4267.27 Å with relative strengths 3:2 in *LS* coupling; this splitting is not detected. We concluded that in NGC 3918 there is no contaminating line of intensity 30% that of 4267 Å and offset farther than 0.4 Å in wavelength.

French (1983) showed that carbon abundances could be derived from permitted recombination lines without recourse

TABLE 6

FLUXES ALONG AN EAST-WEST SLIT

Channel	*R*	C II λ4267	C IV λ4658	He I λ4471	He II λ4686	Mg I λ4571
1.....	21.″0 east	...	...	...	31	...
2.....	18.7 east	...	...	...	14	...
3.....	16.5 east	...	...	1.9	19	...
4.....	14.2 east	...	...	3.6	24	1.0
5.....	12.0 east	1.1	...	3.1	28	...
6.....	9.7 east	0.6	1.1	3.9	30	0.3
7.....	7.5 east	0.8	0.9	4.2	31	0.4
8.....	5.2 east	0.51	0.3	3.1	44	0.3
9.....	3.0 east	0.43	0.45	2.7	64	0.34
10.....	0.7 east	0.56	0.44	3.2	63	0.44
11.....	1.5 west	0.55	0.54	3.0	70	0.41
12.....	3.8 west	0.39	0.42	2.9	57	0.39
13.....	6.0 west	0.7	0.5	4.0	38	0.5
14.....	8.2 west	1.0	2.2	5.3	43	0.9
15.....	10.5 west	1.0	2.1	5.0	48	0.8
16.....	12.7 west	0.6:	...	4.6	46	0.9
17.....	15.0 west	...	...	2.3	51	...
18.....	17.2 west	...	...	2.0:	48	...
19.....	19.5 west	...	...	...	57	...
20.....	21.8 west	...	...	...	68:	...

NOTE.—Fluxes are dereddend and put on the scale $I(H\beta = 100)$ via the Hγ flux. In channels 1 and 20, the Hγ flux is 3×10^{-4} the value in channels 10 and 11.

to UV data. Our spectra include C II $3d$–$4f$ λ4267.2, C III $3p\ ^3P$–$3s\ ^3S$ $\lambda\lambda$4647.4, 4650.2, and 4651.4, and C IV $5g$–$6h$ λ4658.9. The last two C III line components are blended with O II $3s\ ^4P$–$3p\ ^4D$, $J = 5/2$–$7/2$ and $1/2$–$1/2$, at 4949.16 and 4950.84 Å respectively. We fitted the blended spectrum from 4645 to 4655 Å to obtain the C III intensity. We used the known wavelengths of C III and O II lines, together with predicted relative intensities of 5:3:1 for C III lines and 4.5:1 for O II lines. The best fit implied that the C III multiplet contributed 73% of the total flux between 4645 and 4655 Å in the narrow-slit spectrum summed over all 20 spatial channels (run 11). These spectra also include the $5g$–$6h$ lines of N IV and O IV near 4600 Å, which are analogous to the C IV 4658 Å line.

The spectrum in the region from 4615 to 4650 Å is shown in Figure 2. This region also includes the C IV recombination line, [Ar V] λ4625, which is used as a diagnostic for electron temperature, and N III lines around 4640 Å which are excited in the Bowen fluorescence mechanism. The C IV line is important, as it is the only diagnostic of the C^{+4} abundance available. It may be belended with [Fe III] λ4658 in some PNs, but for NGC 3918 we found an upper limit of 20% of the total flux due to [Fe III] from the absence of other lines such as 4702 Å together with the predicted emissivities of Garstang, Robb, and Rountree (1978).

ii) *SAAO Spectra*

Spectra at five different positions in the nebula were obtained in 1982 February and July with the Reticon photon-counting system at the 1.9 m telescope of the SAAO. The dispersion used was 30 Å mm^{-1}, and the range 3400–4400 Å was covered with two grating settings. The resolution of 1 Å enabled the O II $\lambda\lambda$3726/3729 doublet to be resolved. Flux calibration was made through the standards LTT 3864 & 4364 (Stone and Badwin 1983). The best high-dispersion exposures from different positions were merged and averaged, and the mean fluxes from these spectra are given in Table 7.

iii) *AAT Red Spectra*

NGC 3918 was observed on 1984 May 20, with an IPCS detector and the RGO spectograph on the AAT. The observations were described by Clegg and Walsh (1985). The spectra cover the range 5480–6040 Å at a resolution of 1.0 Å, and in the two-dimensional format each spatial channel is separated by 2.″3. Fluxes were put on a scale relative to Hβ via the He I λ5876 line as described by Clegg and Walsh. Many weak lines were detected in these spectra. Table 8 gives a list of all lines measured and their fluxes, corrected for reddening with $c = 0.43$ and on the scale $I(\mathrm{H}\beta) = 100$. These measurements are from the total split spectrum, summed over 20 spatial channels (the extent of detected He I emission is 46″). The strongest line is 4876 Å, and the weakest lines measurable had a flux $\sim 10^{-3}$ that of 5876 Å.

The nine longest wavelength lines belong to a Rydberg series of He II, $n \rightarrow 5$, seen from $n = 20$–28. The C IV lines near 5800 Å are from multiplet 1, $3s^2S$–$3p^2P^o$, and are seen especially when the C IV $2s^2S$–$3p^2P^o$ resonance line at 312 Å is optically thick. The four N II lines near 5680 Å belong to multiplet 3, $3s^3P$–$3p^3D^o$; they are excited by radiative recombination and were used by Wilkes *et al.* (1981) to obtain the N^{++} abundance in NGC 3242. Analysis of the C IV and N II lines is given in § III*d*, and a table of CNO recombination lines used in this paper is also given there.

The sodium D lines are seen in absorption in these spectra. The equivalent widths of the $^2S_{1/2}$–$^2P_{1/2,3/2}$ components were measured to be 200 and 398 mÅ respectively, with an error of $\sim$20%. The derived column density is 2×10^{12} cm^{-2} in the weak-line approximation (thought to be valid since the ratio of equivalent widths is 2:1 and by reference to the curve of growth for Na I toward ζ Oph; Spitzer and Jenkins 1975). The radial velocity of the absorption components in the *nebular* frame of reference was found by comparing the observed Na I and He I λ5876 wavelengths with laboratory vacuum wave-

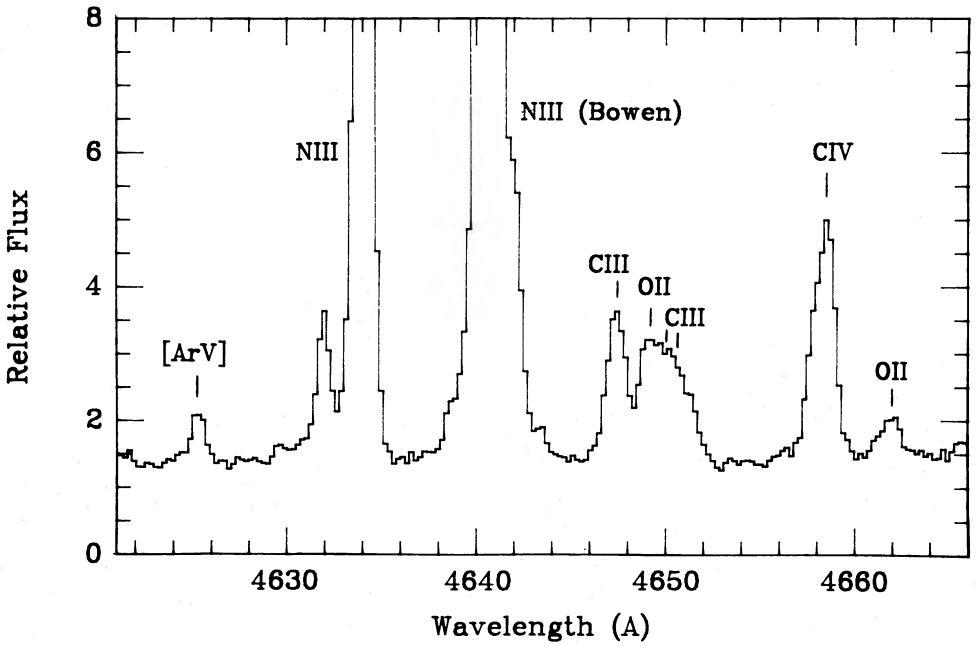

FIG. 2.—Part of the AAT IPCS high-dispersion spectrum, summed over all spatial channels. The N III lines are excited in the Bowen fluorescence mechanism. Fluxes of the blended C III lines were extracted using a fitting procedure (see text).

lengths. Adopted values of the latter were 5891.58, 5897.55 and 5877.29 Å respectively; the value for He I is a mean over three components. The radial velocities of the Na I D1 and D2 lines are +23 and +15 km s^{-1}, both +8 km s^{-1}, in the *nebular* frame. (The radial velocity of the nebula is −16 km s^{-1} [heliocentric] or −24 km s^{-1} [LSR]; Schneider *et al.* 1983). Some of the Na I absorption could come from an expanding neutral shell just outside the nebula: the maximum expansion velocity of NGC 3918 in [O II] is 25 ± 4 km s^{-1}, close to the mean velocity for the D lines of +19 ± 8 km s^{-1}. However, toward an object 1.5 kpc from the Sun (our adopted distance for NGC 3918) and only 4° from the Galactic plane, Na I absorption of this strength can easily be produced in intervening diffuse clouds (see Hobbs 1974).

TABLE 7

SAAO HIGH-RESOLUTION SPECTRA

λ (Å)	Identification	$f(\lambda)$	$I(\lambda)$
3563.....	O IV?	0.303	3.8
3684.....	...	0.264	0.74
3669.....	H I	0.261	0.4:
3670.....	H I	0.261	0.5:
3673.....	H I	0.260	0.6:
3676.....	H I	0.260	1.0:
3679.....	H I	0.259	0.6
3682.....	H I	0.259	0.7
3686.....	H I	0.258	0.80
3688.....	C IV?	0.258	0.24
3691.....	H I	0.257	0.90
3696.....	H I	0.257	1.3
3703.....	H I + He I	0.255	1.6
3707.....	O III	0.255	0.2
3711.....	H I	0.254	1.6
3721.....	H I + [S III]	0.253	3.7
3726.....	[O II]	0.252	53.
3729.....	[O II]	0.251	29.
3734.....	H I	0.250	2.47
3749.....	H I	0.248	2.64
3754.....	O III	0.247	0.75
3757.....	O III	0.246	0.16
3759.....	O III	0.246	3.3
3768.....	He II	0.244	0.2:
3770.....	H I	0.244	3.70
3780.....	He II	0.242	0.16
3789.....	O III	0.241	0.2:
3792.....	O III	0.240	0.2:
3797.....	H I	0.239	5.21
3812.....	He II	0.237	0.32
3819.....	He I	0.235	1.1
3834.....	H I	0.232	6.9
3845.....	...	0.230	0.2
3858.....	He II	0.228	0.34
3868.....	[Ne III]	0.226	138.
3888.....	H I + He I	0.222	18.4
3895.....	...	0.221	0.2:
3923.....	He II	0.215	0.33
3926.....	He I	0.214	0.13
3949.....	...	0.210	0.17
3964.....	He I	0.207	0.90
3966.....	[Ne III]	0.207	42.
3970.....	H I	0.206	15.9
3973.....	...	0.205	0.22
4026.....	He I + He II	0.194	2.65
4068.....	[S II] + C III	0.185	2.25
4072.....	O II + [Fe V]	0.184	0.17
4076.....	[S II]	0.184	0.63
4097.....	N III	0.179	2.4
4101.....	Hδ	0.178	27.1
4120.....	He I	0.174	0.25
4143.....	He I	0.169	0.22
4152.....	C III	0.167	0.09
4156.....	C III	0.166	0.07:
4162.....	C III	0.165	0.09
4187.....	C III	0.159	0.17
4190.....	O II?	0.159	0.1:
4192.....	...	0.158	0.15
4200.....	He II	0.156	0.95
4227.....	[Fe V]	0.150	0.17
4267.....	C II	0.141	0.48
4340.....	Hγ	0.124	47.0
4363.....	[O III]	0.119	21.0

iv) *FORS Red Spectrum*

A spectrum of NGC 3918 in the wavelength region 6000–10,000 Å was taken at the AAT with the faint object red spectrograph (FORS) on 1984 June 11. The FORS consists of a low-dispersion spectrograph with a two-dimensional CCD detector. We obtained a two-dimensional spectrum which has a resolution of ~20 Å. We observed the stars HD 104893 to correct for atmospheric absorption and LTT 4364 as a flux standard. Because of problems with clouds, it was not possible to obtain an absolute calibration of the line intensities, but we were able to measure relative fluxes, as a standard star was observed. We converted the relative fluxes, listed in Table 9, to the scale Hβ = 100 via the Hα + [N II] lines near 6560 Å using the sum of the Hα and [N II] dereddened fluxes from the TPP

TABLE 8

LINE FLUXES IN AAT RED SPECTRA

λ (Å)	Identification	$f(\lambda)$	$I(\lambda)$
5470.3.....	C IV?	−0.143	...
5484.6.....	[Fe VI]	−0.145	0.035
5517.5.....	[Cl III]	−0.151	0.40
5537.7.....	[Cl III]	−0.154	0.56
5571.7.....	O V?	−0.160	0.010
5577.5.....	[O I]	−0.161	0.055
5592.3.....	O III	−0.164	0.073
5597.0.....	O V?	−0.165	0.015
5630.9.....	[Fe VI]	−0.170	0.043
5660.1.....	...	−0.175	0.015
5666.3.....	N II	−0.176	0.010:
5676.6.....	[Fe VI] + N II	−0.178	0.049
5679.8.....	N II	−0.179	0.026
5685.8.....	N II	−0.179	0.009:
5720.9.....	[Fe VII]	−0.185	0.074
5754.3.....	[N II]	−0.191	1.30
5768.5.....	...	−0.193	0.009:
5775.9.....	...	−0.194	0.011
5789.3.....	...	−0.197	0.021
5801.1.....	C IV	−0.198	0.142
5812.0.....	C IV	−0.200	0.078
5832.6.....	...	−0.204	0.019
5846.7.....	...	−0.206	0.016
5867.7.....	...	−0.209	0.105
5875.6.....	He I	−0.210	9.4
5881.9.....	He II (28)	−0.211	0.017
5897.0.....	He II (27)[a]	−0.214	0.018
5913.0.....	He II (26)	−0.217	0.035:
5931.5.....	He II (25)	−0.219	0.038
5953.0.....	He II (24)	−0.223	0.036:
5976.6.....	He II (23)	−0.227	0.032
6004.6.....	He II (22)	−0.231	0.049
6036.6.....	He II (21)	−0.236	0.055
6073.8.....	He II (20)	−0.242	...

NOTE.—The number in parentheses for He II lines is the principal quantum number n for the n^2H^0–5^2G recombination line series whose limit is at 5695 Å.

[a] Affected by interstellar Na I absorption.

TABLE 9

AAT FORS LINE FLUXES[a]

λ (Å)	Identification	Relative Flux	FWHM (Å)	$f(\lambda)$	$I(\lambda)$
5876.....	He I	0.58[b]	21	−0.211	...
6300.....	[O I]	0.28[b]	13	−0.276	...
6363.....	[O I]	0.08[b]	10	−0.285	...
6565.....	[N II] + Hα	14.3	26	−0.314	344
6678.....	He I	0.07	12	−0.330	1.7
6724.....	[S II]	0.28	21	−0.336	6.5
7006.....	Ar V	0.11	11	−0.373	2.5
7065.....	He I	0.17	18	−0.380	3.8
7136.....	Ar III	0.82	18	−0.389	18.2
7237.....	C II + Ar IV	0.59	16	−0.401	13.0
7263.....	Ar IV	0.08	10	−0.404	1.9
7325.....	[O II]	0.51	25	−0.411	11.2
7477.....	...	0.04	16	−0.428	0.88
8751.....	H I Pa12?	0.18	16	−0.549	3.5
8793.....	...	0.37	12	−0.552	7.1
9069.....	[S III]	1.03	20	−0.574	19.0
9531.....	[S III]	4.18	21	−0.606	75.0

[a] Observed and dereddened.

[b] Affected by night sky emission; not used for analysis.

data. Because it was not possible to make an accurate sky subtraction, lines such as [O I] λ6300 and He I λ5876 were not used from this spectrum; these lines are contaminated by night sky lines of [O I] and Na I respectively.

The measured ratio of [S III] λλ9532/6069 lines was found to be 3.9, in disagreement with the theoretical ratio of 2.8 (calculated from the *A*-values given by Mendoza 1982). We interpreted this as due to absorption of the λ9069 line by telluric water vapor lines and used only the [S III] λ9532 flux for analysis.

c) *Images of NGC 3918*

A fundamental requirement for modeling is the ability to match the observed map on the sky of the nebula in a line such as Hβ which traces the distribution of hydrogen ions. We were fortunate to have access to unreduced electronographic images of NGC 3918, taken with the 1.5 m telescope at the Boyden Observatory, South Africa, in 1973 by Drs. K. Reay and S. P. Worswick, who gave us permission to trace them. Their observing methods and the electronographic camera were described by Coleman, Reay, and Worswick (1975). The images recorded on L4 emulsion were two 30 minute exposures in Hβ light and two 5 minute exposures in [O III] λ5007. The plate scale was 8″.8 mm^{-1}. We traced these four plates with the PDS microdensitometer at the Royal Greenwich Observatory, using a 24 μm entrance aperture (corresponding to 0.25 $arcsec^2$ projected on the sky).

The digital images thus obtained were processed with software written by Dr. S. Hart for the UK STARLINK system. Contour maps of the best exposed image in each line were made. The final maps were smoothed with a filtering technique to a resolution of 1″. The Hβ map is shown in Fig. 3. Images of the nebula in Hβ and [O III] light have a fairly smooth appearance, with approximate circular symmetry.

We were also able to superpose, interactively on a graphics screen, a digital mask having the shape of the *IUE* large aperture and, by multiplying image and mask together, to determine the fraction of the total nebular Hβ flux falling within the LAP. It was found that, for any position angle of the LAP, this

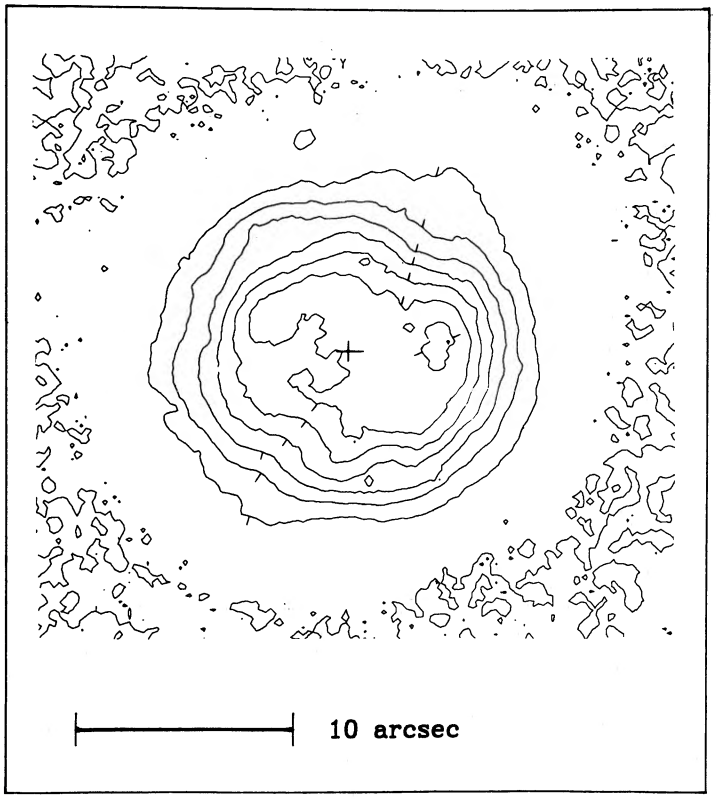

FIG. 3.—Linear contour map in Hβ light. Contours are given at eight equally spaced levels. The outer structure represents the plate noise. Tick marks are placed on the low-intensity side of contour lines. The cross shows our adopted position of the nebular center.

fraction was $f = 0.80 \pm 0.04$ when the aperture is positioned on the apparent nebular center.

The average Hβ radial profile was found by measuring the variation of intensity on the map in Hβ light in eight different radial directions. The central star of NGC 3918 was not detected, and the nominal nebular center was chosen as the apparent center of the outer, most circular contours. The mean Hβ profile is shown in Figure 4, together with the profile from the best fitting composite photoionization model (described in § V).

d) Coudé Spectrum in [O III] *Lines*

A high-resolution two-dimensional spectrum of NGC 3918 was kindly taken for us by Drs. P. R. Wood and M. S. Bessell, with an echelle and 32 inch (81 cm) camera at the coudé focus of the 1.9 m telescope of the Mount Stromlo Observatory in 1983 June. The detector was a two-dimensional photon counting array, and the entrance slit of width 300 μm (1".2 projected on the sky) was placed east-west across the center of the nebula. The exposure time was 1200 s. Wavelength and flux calibrations were achieved through exposures of an iron arc and of the star HD 140283. The projected slit length was 17", and each pixel corresponded to 0".89 along the slit. The velocity resolution (FWHM of arc lines) was 5.6 km s^{-1}. Spectra of the [O II] lines at 3726 and 3729 Å were measured as a function of position along the slit. [O II] emission was detected from 21 positions, out to a radial distance 8".9 east and west of center.

Part of the two-dimensional image, around the [O II] line components, is shown in Figure 5 (Plate 15). The splitting of each component due to nebular expansion is visible, and the absence of emission at the ends of the slit (near the systemic velocity of the nebula) is striking. Figure 5 can be compared with slit spectra showing splitting displayed by Osterbrock (1974). The usual "double-bowed" lines are seen but with the "ends" missing and with the blueshifted components stronger. The conclusions are that most of the O^+ ions are concentrated toward the front and rear of the object (where the positive and negative Doppler shifts are largest), and that there are more O^+ ions on the near side. (An alternative explanation for the asymmetry was proposed by Pena and Torres-Peimbert 1985, who suggested that emission from the far side was attenuated by dust within the nebula).

The image displayed in Figure 5 has been flux-calibrated and rotated so that the direction of dispersion lies parallel to one axis of the two-dimensional data "frame." Individual cross sections (cuts at constant spatial position) were measured. In each cut the ratio of the 3726 to 3729 Å flux indicates the projected electron density at that position. Results for $N_e(O^+)$ along the slit are shown in Figure 6, together with the predictions of the composite model described in § V. In the figure the two points at each radius correspond to the measurements east and west of the center. Values of N_e are for an assumed temperature $T_e = 10{,}000$ K (although they are quite insensitive to the assumed T_e). Within the errors, there are no significant

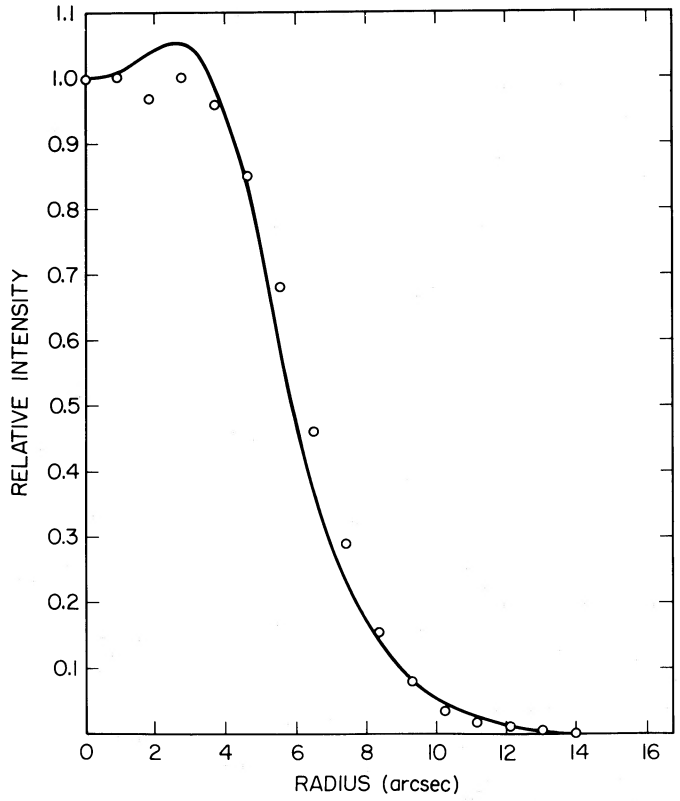

FIG. 4.—Mean radial profile in Hβ light. The points denote the average radial intensity of Hβ, normalized to the central intensity, while the curve shows the prediction of the adopted composite model.

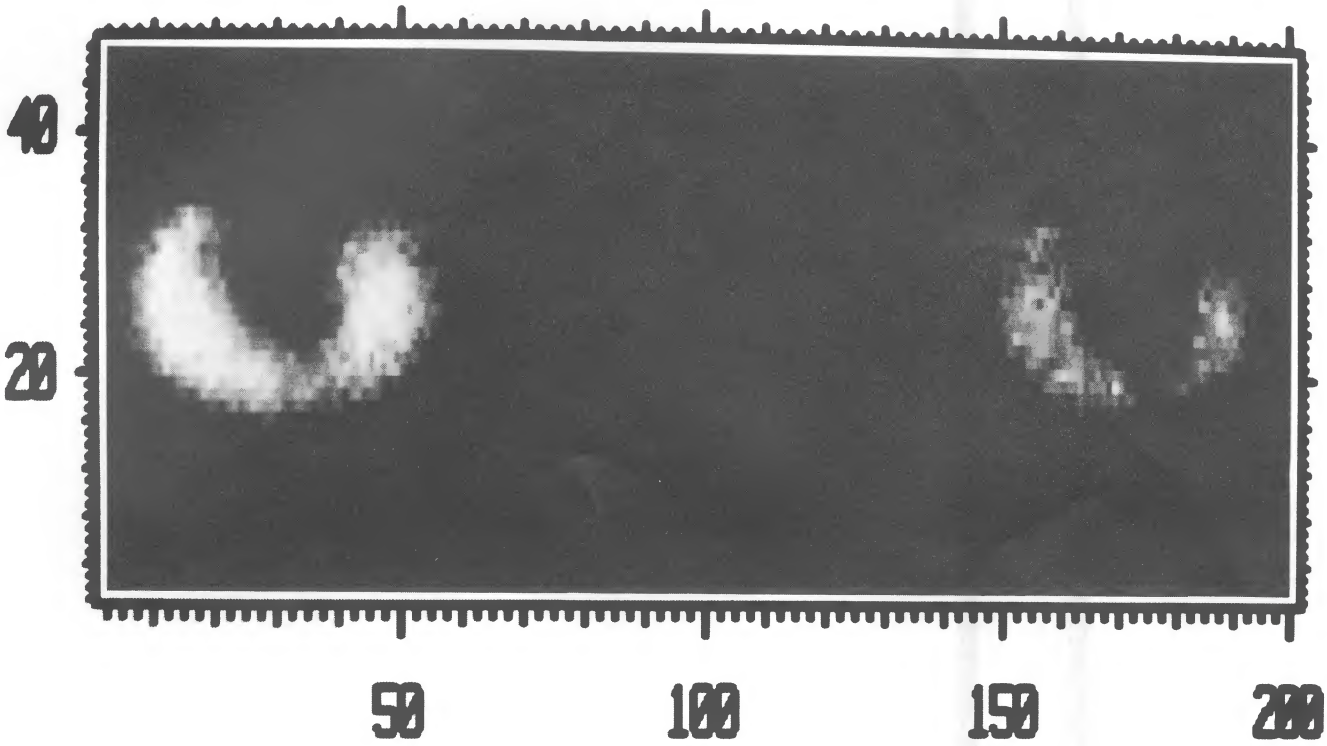

FIG. 5.—Coudé velocity-position map of the [O II] lines λλ3726.1, 3729.2. *Horizontal axis*, wavelength (or velocity) with the scale 1.6 km s^{-1} per channel. *Vertical axis*, position along east-west slit, with the scale 0″.89 per channel. The λ3726 line (seen on the left) is about twice as strong as 3729 Å because the electron density $N_e = 4500$ cm^{-3}. Each line is split by the expansion velocity, with a maximum splitting of 50 km s^{-1} near the center of the object. Note the absence of emission near the edges and the slight tilt of the line of mean velocity along the slit.

CLEGG, HARRINGTON, BARLOW, and WALSH (*see* page 558)

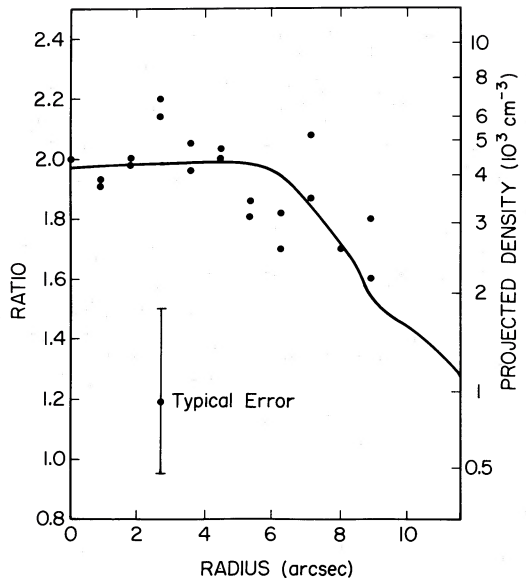

FIG. 6.—Projected densities along an east-west slit across NGC 3918, from the [O II] λ3726/λ3729 ratio. At each radius except the center, the two dots mark the measured ratios to the east and west of center. The solid line shows the predicted variation of the projected ratio in the final composite model (the absolute values have been scaled up by 17%).

differences between derived values of N_e for the front and rear parts of the nebula.

The spectral cross section through the nebular center shows a complete lack of emission around zero velocity. The separation between the peaks of the velocity components was measured to be 0.634 and 0.635 Å for the 3726 and 3729 Å lines respectively. The maximum expansion velocity for O^+ ions is then 25 ± 4 km s^{-1}. The mean radial velocity of the blue and red components varies systematically by 8 km s^{-1} from the east to west edge of NGC 3918, as seen from the "tilt" of $\sim 15°$ of the bowed components in Fig. 5. Such a tilt is usually interpreted in terms of an expanding spheroid, one of whose axes is offset from the line-of-sight direction (e.g., Weedman 1968). In the present case, it may arise from quite modest departures from spherical symmetry, and the angle between the line of sight and the major axis of the spheroid (assumed here to be prolate) may be small. For example, Sabbadin (1984) found a tilt for NGC 6309 for which the mean radial velocity of the blue and red components varied by about ~ 10 km s^{-1} across the nebula; this was fitted by a prolate spheroid of axial ratio 1.2:1 whose major axis was inclined at only 15° to the line of sight.

In addition, Figure 5 shows that the [O II] emission is maximum at the largest positive and negative velocities. Together with the roughly circular symmetry seen in the Hβ and [O III] images, this suggested to us a structure which is a solid of revolution seen almost end-on. Such a geometry is considered further in § V.

III. NEBULAR ANALYSIS

a) *The Reddening*

We evaluated the interstellar reddening constant $c(\mathrm{H}\beta)$ from five methods: decrements of H I and He II lines, the 2200 Å feature, comparison of radio and Hβ fluxes, and the ratio of [O II] lines.

The absolute Hβ flux, in ergs cm^{-2} s^{-1}, has been given for the whole object as $\log F = -10.01 \pm 0.02$ (Webster 1969), -10.03 ± 0.01 (KM), -10.05 (Carrasco, Serrano, and Castero 1983), and -10.03 (TPP). We corrected for the contribution of the He II 8–4 line from the measured He II λ4686 line and adopted $\log F = -10.03 \pm 0.02$. The radio flux at 5 GHz was measured by Milne and Aller (1975): $S = 0.86 \pm 0.06$ Jy. The measurements of Milne and Aller at 14.7 GHz and of Milne and Webster (1979) at 2.7 GHz indicate that the nebula is optically thin at 5 GHz. We then used the expressions of Milne and Aller to evaluate c with the parameters $y^+ = 0.071$, $y^{++} = 0.032$, and $T_e(\mathrm{H}^+) = 12{,}000$ K. [In this paper we use $y^+ = N(\mathrm{He}^+)/N(\mathrm{H}^+)$ and $y^{++} = N(\mathrm{He}^{++})/N(\mathrm{H}^+)$.]

The reddening was also evaluated from the ratios of the lines Hα, Hβ, and Hγ together with the predicted ratios from Brocklehurst (1971), and from the ratios of He II lines at 4686, 3204, 2512 and 1640 Å, together with the predicted intensities from Seaton (1978) for the case $T_e(\mathrm{He}^{++}) = 14{,}000$ K. We note that the expected electron temperature for He II lines may be considerably higher than for H I lines. We did not use the He II λ2733 flux, as this line was difficult to measure above the strong continuum at this wavelength. The adopted He II fluxes are 38.2 (λ4686), 9.25 (λ3204), 2.50 (λ2512), and 87.5 (λ1640), in units of 10^{-12} ergs cm^{-2} s^{-1}. It was assumed that the *IUE* LAP included the same fraction (0.8) of the nebular He II emission as it did of Hβ emission; errors introduced by this are discussed below. We also dereddened the continuum observed with the *IUE* with the extinction curve of Seaton (1979), varying c so as to nullify the λ2200 feature. Lastly, we used the ratio of [O II] λλ2470, 7330 lines arising from the same upper level, with the A-values of Zeippen (1982).

Results of these methods are given in Table 10. There is generally good agreement between the methods, suggesting that the reddening law toward NGC 3918 follows the average law. Values of c from the Balmer decrement are systematically lower than our adopted value, regardless of whether the H line fluxes of TPP, KM, or § II are used. However, the Balmer decrement value is, within the errors, not inconsistent with our adopted value of $c = 0.43 \pm 0.05$. This is close to the value adopted by Pena and Torres-Peimbert (1985) of $c = 0.40$.

Evidence of interstellar absorption by H Lyα was seen on the *IUE* low-resolution image SWP 18029, in which the continuum is well exposed. In Figure 7 the normalized, dereddened continuum is compared to Lorentzian profiles of a Lyα absorption line, calculated for column densities $N(\mathrm{H\ I}) = 1.8$ and 5.0×10^{21} cm^{-2} on the assumption of a pure damping profile. The best fit is for a column of 2×10^{21} cm^{-2} with an uncertainty of 60%. The ratio $N(\mathrm{H})/E(B-V)$ is then $6 \pm 4 \times 10^{21}$ cm^{-2}, not very different from the average ratio found toward 75 stars by Bohlin, Savage, and Drake (1978): 4.8×10^{21} cm^{-2}. The ratio of column densities of interstellar Na I (§ II*b*[iii]) and H I is then 1.1×10^{-9}, a value somewhat

TABLE 10

VALUES OF REDDENING CONSTANT $c(\mathrm{H}\beta)$

Method	Result
Radio–Hβ fluxes	0.43 ± 0.04
Balmer decrement	0.33 ± 0.14
He II λλ1640–4686	0.45 ± 0.06
He II λλ1640–3204	0.41 ± 0.10
2200 Å feature	0.4 ± 0.2
[O II] λλ7330–2470	0.41 ± 0.10
Adopted	0.43 ± 0.05

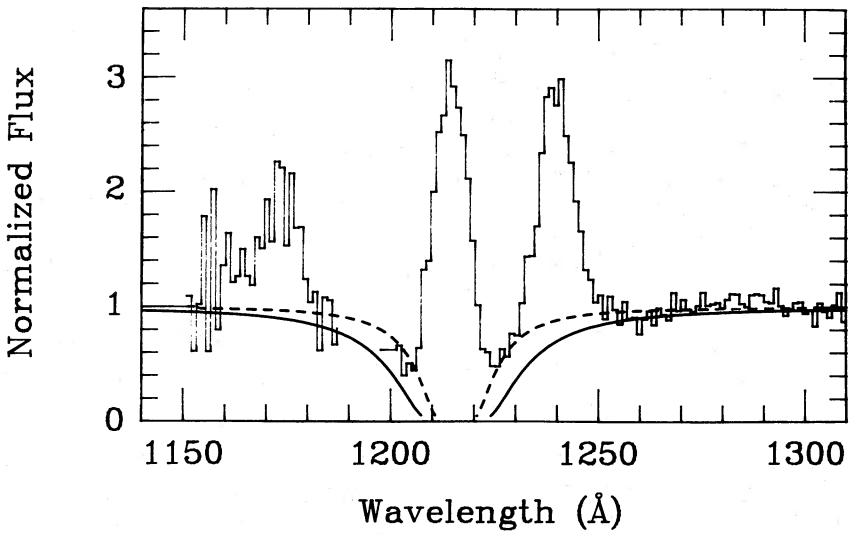

FIG. 7.—Part of the low-dispersion *IUE* image SWP 18029. The continuum has been dereddened and normalized to unity. The dashed and solid curves show fits to the wings of interstellar Lyα for columns $N(\mathrm{H}) = 1.8$ and 5.1×10^{21} cm^{-2} respectively. The emission lines are C III λ1176, geocoronal Lyα, and N V λ1240.

lower than the average ratio of 4×10^{-9} given by Hobbs (1974). The fit shown in Figure 7 also gives guidance for the measurement of C III λ1176 and N V λ1240 line fluxes.

b) *Adopted Fluxes*

Using the above results for the reddening and the fraction f of the nebular flux in the *IUE* LAP, we compiled a set of adopted fluxes which are intended to be representative of the whole nebula. For the *IUE* data we assumed that f had the same value for all ions. This was because the measured line ratios given in Table 6 indicate that ionic ratios are surprisingly constant over the surface of the nebula. For example, the ratio He II λ4686/Hβ only varies by a factor of 2 across the nebula. This is as if the He^+ Strömgren sphere edge were not detected, which seems difficult to reconcile with the low He II λ4686/Hβ ratio of 0.46. (The resolution of this problem is given in § V). For the optical data, a careful assessment was made from our own spectra and those of KM and TPP to find representative fluxes. In the infrared, the *IRAS* low-resolution spectrometer spectra (Pottasch *et al.* 1986) are for the whole PN. The IR line fluxes from Beck *et al.* (1981) are for a 7″ beam and cannot easily be cast relative to Hβ; they are not used in this analysis.

Some error is introduced by our assumption of constant f for all ions. We calculated f(He II) from the dereddened flux of 1640 Å in the *IUE* LAP and the total λ4686 flux; this gave $f = 0.73 \pm 0.08$. The slit spectra (Table 6), however, suggest that He II lines are slightly stronger relative to Hβ near the nebular center, which would yield a value for f larger than 0.8. There are uncertainties of $\sim$12% in *IUE* line fluxes from the aperture correction in general. For lines of the highest ionization stages, such as Mg V and O V, the uncertainty is probably 15% (f may be close to unity for these lines).

Table 11 shows the adopted UV fluxes. Observed and dereddened values in the *IUE* LAP are listed, plus dereddened fluxes for the whole nebula on the scale $I(\mathrm{H}\beta) = 100$.

c) N_e *and* T_e *Diagnostics*

The line ratios used for measurement of electron density and temperature for different ions are listed in Table 12, together with a comparison between observed ratios and those predicted from our model. Especially for the density diagnostics, we compared the model ratios directly with observed values, because the nominal values of N_e deduced from observations cannot be directly compared with a model in which a variable density law $N(R)$ is used. The atomic data are taken from the compilation by Mendoza (1982) with the exception of Si III (Dufton, Keenan, and Kingston 1984), O IV (Hayes and Nussbaumer 1983), and Mg I (H. E. Saraph, private communication). The result for N_e(Cl III) was obtained with the prescription of Saraph and Seaton (1970), and we note that use of their recipe brings this result into good agreement with

TABLE 11

ADOPTED ULTRAVIOLET FLUXES
(10^{-2} ergs cm^{-2} s^{-1})

λ (Å)	Identification	F(obs.)	F(dered.)	$F(\mathrm{H}\beta = 100)$
1176.....	C III	3:	50:	25:
1240.....	N V	6.7	91	46
1342.....	O IV	0.4:	4:	2:
1399.....	Si IV	1.8	18	9.3
1401.....	O IV]	8.0	78	40
1486.....	N IV]	10.8	98	50
1550.....	C IV	117	1010	514
1576.....	C III + [Ne V]	1.3	11	5.6
1602.....	Ne IV	1.1	13	6.6
1640.....	He II	70	580	295
1664.....	O III]	8.3	68	35
1751.....	N III]	7.0	57	29
1886.....	Si III]	1.8	15	8
1908.....	C III]	117	1020	540
2254.....	He II	0.43	5.3	2.7
2297.....	C III	0.9:	9.9:	5:
2307.....	He II	0.58	6.3	3.2
2321.....	[O III]	2.2	23	11.5
2326.....	C II	6.6	68	34
2423.....	[Ne IV]	32	260	132
2470.....	[O II]	2.4	18	9.0
2733.....	He II	4.5	24	12
2783.....	Mg V]	2.1	11	5.6
2837.....	O III	4.1	20	10.2
3133.....	O III	39	170	85
3204.....	He II	7.4	30	15

TABLE 12

N_e AND T_e DIAGNOSTIC RATIOS

Ion[a]	Lines (Å)	Ratio	Result[b]	Model Ratio[c]
		N_e		
Mg I	4562/4571	0.19	9500:	0.42:
S II	6716/6731	0.55	5700	0.70
O II	3726/3929	1.98	4600	1.61
C III	1906/1909	1.31	6400	1.36
Si III	1883/1892	1.37	3500	1.30
Cl III	5518/5538	0.71	4000	...
Ne IV	2421/2424	1.00	5000	0.93
N IV	1483/1486	1.85	<10000	1.87
O IV	1401/1404	1.50	≥ 7000	1.14
		T_e		
O I	5577/6300	0.013	10000	0.020
N II	5755/6584	0.017	9800	0.025
C III	4267/1908	0.0008	11400	0.0005
S III	6312/9532	0.032	12500:[d]	0.029
O III	4363/5007	0.013	12400	0.013
Ar V	4625/7006	0.020	13000	...
Ne IV	1602/2423	0.047	14600	0.049
Ne V	1575/3426	0.007:	14000:[e]	0.012

[a] In order of increasing ionization potential.
[b] N_e in cm^{-3} $\pm$ 50%; T_e in K $\pm$ 2000 K except where noted.
[c] Described in § V.
[d] $\pm$1500 K (the λ9532 line may be affected by telluric absorption).
[e] $\pm$2000 K.

other diagnostics. Typical errors are $\pm$1200 K for T_e and $\pm$50% for N_e, resulting from 20% errors in measured ratios.

A number of recombination lines from C, N, and O are analyzed below (§§ III*c* and III*d*), and they are summarized in Table 13.

The ratio of carbon lines $I(4267)/I(1908)$, yielding $T_e(C^{++})$, is extremely sensitive to temperature, and we note that the resulting value of 11,400 $\pm$ 700 K is intermediate between values of $T_e(N^+)$ and $T_e(O^{++})$, as might be expected from their respective ionization potentials. The total C II λ4267 flux in this PN is not significantly anomalous, in view of the typical errors in the temperature determinations. The value of $T_e(C^{++})$ is 1000 K lower than that of S^{++} (with the same ionization potential), but the S^{++} value is based on a line at 9532 Å which is susceptible to absorption by telluric water lines.

TABLE 13

CNO RECOMBINATION LINES ANALYZED

Spectrum	λ (Å)	Transition	Type[a]	Reference for Rate
C II	4267	$3d^2D$–$4f^2F^o$	R	1
C III	1577–1578	$3d^3D$–$3d'^3F^o$	D	2
	2297	$2p^1P^o$–$2p^2\,^1D$	D	2
	4647–4651	$3s^3S$–$3p^3P^o$	R, D	1, 2
C IV	4658	$5g^2G$–$6h^2H^o$	R	1
	5801–5812	$3s^2S$–$3p^2P^o$	R	3
N II	5680	$3s^3P^o$–$3p^3D$	R	4
N IV	1718	$2p^1P^o$–$2p^2\,^1D$	D	2
	4606	$5g^3G$–$6h^3H^o$	D, R	2, 5
O IV	1342	$2p^2\,^2P$–$2p^3\,^2D^o$	D	2
	4632	$5g^2G$–$6h^2H^o$	R	5

[a] Excitation by radiative (R) or dielectronic (D) recombination.

REFERENCES.—(1) Pengally 1963, quoted by Seaton 1977. (2) Nussbaumer and Storey 1984. (3) Calculated by P. J. Storey, see § III*d*. (4) Wilkes *et al.* 1981. (5) For N IV and O IV 5*g*–6*h* lines we used the recombination coefficient from ref. (1) for C IV 5*g*–6*h*, evaluated at 16,000 K. For the N IV line we also included the dielectronic rate of ref. (2).

Values of N_e and T_e for different ions need not be identical, since the different species sample different regions of the nebular volume. For high-excitation PNs, ions such as N^+, S^+, and O^+ are not very representative, but the *IUE* cameras fortunately provide diagnostics from Si^{++}, C^{++}, and O^{+3}. We draw attention to the possibility of obtaining N_e and T_e for the highly ionized part of the nebula from fluxes of [Ne IV] $\lambda\lambda$1602, 2421, and 2423. Figure 8 shows the solution for $N_e(Ne^{+3})$ and $T_e(Ne^{+3})$ from these lines. Since the ionization potential of Ne^{++} is 63.4 eV, these measurements refer to the He^{++} zone of the object. The line ratio $I(1575)/I(3426)$ for $T_e(Ne^{+4})$ must be used with great caution, because the λ1575 line is weak and is blended with C III dielectronic recombination lines near 1577 Å. This ratio appears to be the temperature diagnostic from the highest ionization stage currently accessible. We subtracted the expected contribution of C III λ1577, calculated from the observed C III λ2297 flux and the recombination coefficients of Nussbaumer and Storey (1984), from the total λ1577 flux. (The $\lambda\lambda$1575, 1577 lines were not detected in our high-resolution *IUE* spectra). Over 80% of the total flux is due to C III and not to [Ne V] in this object.

d) Abundances

We obtained empirical abundances for 11 elements. Since TPP and Torres-Peimbert, Pena, and Daltabuit (1981) have previously derived abundances for some of these species, our discussion of the derivations is highly abbreviated. The lines used, adopted fluxes, and resulting ionic abundances are given in Table 14. The atomic data used are from Mendoza (1982) with the exceptions noted in § III*c*. For each ion, a value of $N_e = 4500$ cm^{-3} was adopted, and a value of T_e used based on the results of Table 12. A statistical equilibrium solution for an n-level atom was then found, from which the observed line flux relative to Hβ is converted to a fractional ionic abundance $N_i/N(H^+)$.

A total iron abundance of Fe/H = 4×10^{-7} was found from the derived sum $(Fe^{+5} + Fe^{+6})/H^+ = 6.8 \times 10^{-8}$ multiplied by an ionization correction factor of 5.5, taken from an ionization model including Fe ions by Shields (1978) for NGC 7027. Although this is a model for a different nebula, NGC 7027 has derived values of He^{++}/He^+ and Fe^{+6}/Fe^{+5} ratios within 20% of the NGC 3918 values, and so we considered this procedure the best available. Note that we used atomic data from Nussbaumer and Storey (1978, 1982) for [Fe VI] and [Fe VII]. The line flux ratio R(5631 Å/5677 Å) for [Fe VI] is in agreement within the errors with the predicted emissivities. The total Fe/H ratio is uncertain to at least a factor of 2. The strengths of the [Fe VI] and [Fe VII] lines in NGC 3918 are $\sim$4 times lower than those for NGC 7027, which leads to a much lower abundance (Fe/H 0.01 the solar value). However, the [Fe V] λ4227 line has about the same strength in the two nebulae ($F = 0.18$, see Table 7). At first this suggested to us that the iron ionic fractions in NGC 3918 were quite different from those in NGC 7027, which was surprising because other ionic ratios such as He^{++}/He^+, N^{+4}/N^{+3}, and Fe^{+6}/Fe^{+5} are very similar. (The IP of N^{+3} is the same as that of Fe^{+4}). However, the transition probabilities of Garstang (1957) for [Fe V] show that for the λ4227 line, $A = 1.1 \times 10^{-3}$ s^{-1}. No collision strengths are available for [Fe V], but use of $\Omega = 1.0$ yields a critical density

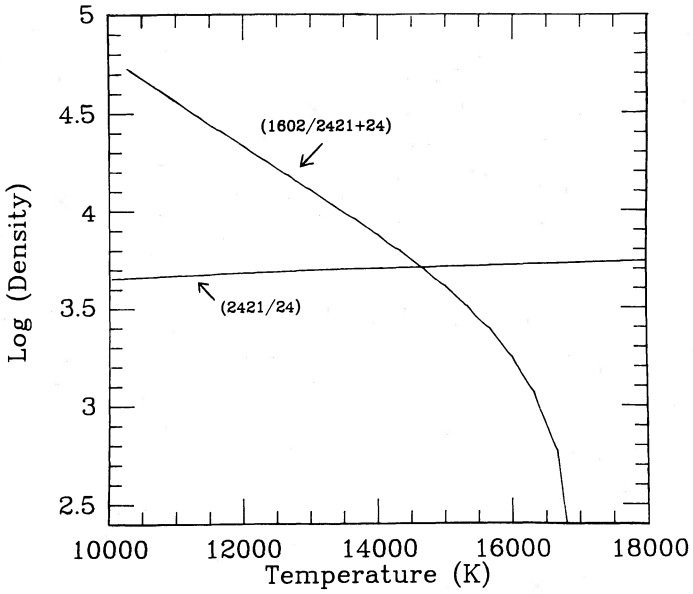

FIG. 8.—Fit diagram for [Ne IV] lines. Ratios of line fluxes at λλ1602, 2421, and 2424 provide measurement of N_e and T_e in the highly ionized part of the nebula.

for 4227 Å of 1.2×10^5 cm^{-3}. Kaler *et al.* (1976) derived an electron density for NGC 7027 from forbidden line ratios: $N_e = 1.2 \times 10^5$ cm^{-3}. We therefore suggest that 4227 Å is collisionally suppressed in NGC 7027 but not in NGC 3918. These effects may need to be taken into account in deriving empirical collision strengths from observed lines in NGC 7027. Note that the [Fe VI] and [Fe VII] lines used here are not collisionally suppressed even at densities of 10^6 cm^{-3}.

Wilkes *et al.* (1981) used permitted recombination lines of N II to obtain the N^{++} abundance in NGC 3242 without recourse to *IUE* data. Detection of these lines and of N III] λ1751 in NGC 3918 provides an opportunity to test this method. Their recommended recombination coefficient for the whole N II λ5680 multiplet, at $T_e = 12{,}500$ K, is 4.3×10^{-13} cm^3 s^{-1}. The summed fluxes in the observed lines then yield an ionic fraction $N^{++}/H^+ = 4.2 \times 10^{-5}$, 40% lower than the value derived from the collisionally excited UV line: $N^{++}/H^+ = 7.2 \times 10^{-5}$ (Table 14). The optical lines were very faint and difficult to measure in our spectra. When both multiplets are observed, the comparison could be regarded as yielding $T_e(N^{++})$. The recombination lines are so weak, though, that they can only be used in the very brightest nebulae.

Detection of several recombination lines of C II, C III, and C IV allows us to obtain a reliable empirical C abundance: $C/H = 1.0 \times 10^{-3}$. This is derived without any need to estimate the attenuation of C IV λ1550 by dust absorption. We were also able to check some empirical formulae proposed for C abundances. TPP suggested that, when no lines of C^{+4} were observed, the formula $C^{+4}/(C^{+3} + C^{+2}) = He^{++}/He^+$ could be used (here, symbols such as C^{+3} denote their fractional abundances). For NGC 3918, the C ratio is 0.31, but $He^{++}/He^+ = 0.6$. Their method overestimates the C^{+4} fraction; the effects of charge-exchange and dielectronic recombination serve to reduce it. Kaler (1982) presented an empirical formula (his eqn. [1a]) for C/H in terms of the line flux $I(4267)$ and the ratio He^{++}/He. For NGC 3918 his equation gives $C/H = 3.4 \times 10^{-4}$, a factor of 3 below the direct value; the relation does not seem to work well for such a high-excitation object as this.

TABLE 14

EMPIRICAL ABUNDANCES

Ion	Line (Å)	$I(\lambda)$	X^i/H^+
He^+	4471	2.8	5.8E−2
	5876	9.4	7.1E−2
	6678	2.2	5.8E−2
He^{++}	4686	45	4.1E−2
C^+	2326	34	5.3E−5
C^{++}	1908	540	5.3E−4
C^{+3}	2297	5:	1.8E−4:
	4650	0.47	2.1E−4
C^{+4}	4658	0.42	2.3E−4
N^0	5200	0.54	7.1E−7
N^+	6584	64	1.3E−5
N^{++}	1751	29	7.2E−5
	5670	0.003:	4.2E−5:
N^{+3}	1486	50	6.6E−5
N^{+4}	1240	46	2.4E−5
	4606	0.065	2.6E−5
O^0	6300	3.8	7.6E−6
O^+	3727	65	2.8E−5
O^{++}	5007	1560	2.8E−4
	1664	35	2.9E−4
O^{+3}	1402	40	2.5E−4
O^{+4}	1342	2:	1.0E−4:
	4631	0.15	8.1E−5
Ne^+	12.8 μ	12:	1.1E−5:
Ne^{++}	3868	120	4.3E−5
	15 μ	88	3.7E−5
Ne^{+3}	2423	132	5.0E−5
Ne^{+4}	3426	80	1.8E−5
	14 μ	48	3.4E−5
Ar^{++}	7136	18.2	1.0E−6
Ar^{+3}	4711	5.6	8.1E−7
Ar^{+4}	7006	2.5	1.8E−7
	4625	0.05	1.4E−7
S^+	6725	6.5	2.5E−7
S^{++}	9532	75	2.7E−6
S^{+3}	10.5 μ	64	1.8E−6
Si^{++}	1885	8	8.4E−7
Si^{+3}	1398	9	2.0E−6
Mg^0	4565	0.41	1.4E−8:
Mg^{+4}	2783	5.6	3.5E−6
Cl^{++}	5528	0.96	3.8E−8
Fe^{++}	4702	<0.03	...
Fe^{+4}	4227	0.17:	...
Fe^{+5}	5485	0.035	3.6E−8
Fe^{+6}	5721	0.074	3.2E−8

Shields (1978) used the C IV λ5812 line to obtain C^{+4} abundances in six PNs with the prescription $C^{+4}/H^+ = 0.17\, I(5812)/I(H\beta)$. In NGC 3918 we observe both C IV $5g$–$6h$ λ4658, which is excited only by recombination (Grandi 1976; Seaton 1978), and $3s^2S$–$3p^2P$ λλ5801, 5812, which are strongly affected by case A/case B assumptions and can perhaps be excited by absorption of starlight (Grandi 1976). We examined the ratio $R(5805/4658)$, where 5805 Å represents the total flux in the multiplet (5801 + 5812 Å). A recombination coefficient onto the C IV $3p^2P$ level was kindly calculated for us by Dr. P. J. Storey. The effective coefficient for a hydrogenic ion of charge 4 was computed for case B (no np–$2s$ transitions

included in the recombination cascade); the method was described by Seaton and Storey (1976). The result for $\alpha_{eff}(3p)$ is $9.2 \times 10^{-13} t_e^{-0.57}$ cm^3 s^{-1} (the value for case A is very similar). Since the branching ratio for (3*p*–2*s*):(3*p*–3*s*) transitions is 144:1 for the *A*-values of Wiese, Smith, and Glennon (1966), the strength of 5805 Å in case A will be very weak. For perfect case B recombination, we predict $C^{+4}/H^+ = 0.04 \times I(5805)/I(H\beta)$. The predicted value of $R(5805/4658)$ is 1.3, rather lower than the observed value of 1.9 ± 0.3. This suggests that there may indeed be a contribution to the 5800 Å lines from fluorescence, which must surely vary from nebula to nebula. Use of these lines is not recommended for abundances if the λ4658 line is available.

In this paper we report the first identification of the N IV and O IV 5*g*–6*h* lines near 4600 Å. Abundances of N^{+4} and O^{+4} found from these lines (Tables 13 and 14) agree with values from UV collisionally excited lines to within 20%.

e) Adopted Distance

Our data do not provide any new distance indicators for NGC 3918. Martin (1981) cites some estimates: 2.0 kpc from the Shklovsky (1956) method, and 0.8 kpc from the synthetic distance scale of Acker (1976). More recently, Pottasch (1982) derived a value of 1.3 kpc from the relation between $E(B-V)$ and distance for stars within a few degrees of NGC 3918, using a reddening constant $c = 0.42$ which is very close to our adopted value. We adopted a distance of 1.5 kpc, and we note that it is probably uncertain to a factor of 2. The model presented in § V has a filling factor of unity, and it reproduces the observed absolute Hβ flux and density diagnostic ratios. Then as far as the model is concerned, the adopted distance is a minimum value: if the distance were less, a filling factor greater than unity would be required, which is unphysical.

IV. THE CENTRAL STAR

The central star of NGC 3918 was not seen directly in any of our observations; the high nebular surface brightness masks the star. We decomposed the observed continuum, from the *IUE* and KM data, into contributions from a hot star and a nebular continuum. The observed UV continuum was obtained by merging several *IUE* SWP and LWR images, choosing from each one wavelength regions where the continuum was well exposed. These merged data, together with the continuum filter measurements of KM, were dereddened with $c = 0.43$. The resulting distribution is shown in Figure 9.

The initial decomposition comprised a theoretical nebular continuum calculated for the case $T_e(H^+) = 12{,}000$ K, $y^+ = 0.071$, and $y^{++} = 0.032$, and normalized to 80% of the absolute Hβ flux for the *IUE* region (1200–3200 Å) and to 100% of Hβ in the visible (since the KM continuum fluxes are for the whole object). The final decomposition shown in the figure used a more detailed calculation from the composite photoionization model. The figure shows that the dereddened continuum is well fitted by the sum of fluxes from a hot star and from the nebular gas.

In this PN, the starlight is severely masked by nebular recombination radiation, and the stellar flux only dominates for wavelengths less than ~1400 Å. This case seems to be that of the most severe masking in which the stellar UV continuum was successfully extracted so far, and it was thought useful to have confirmation that starlight does dominate at the shortest wavelengths. This was provided by measurements of the widths, in pixels perpendicular to the direction of dispersion, of the *IUE* image SWP 18029 in which the continuum is well exposed. Table 15 shows the results: the spectrum narrows considerably for $\lambda < 1500$ Å (much more than the narrowing of the point spread function of the *IUE* SWP camera). This is due to the fact that the nebular continuum arises from an

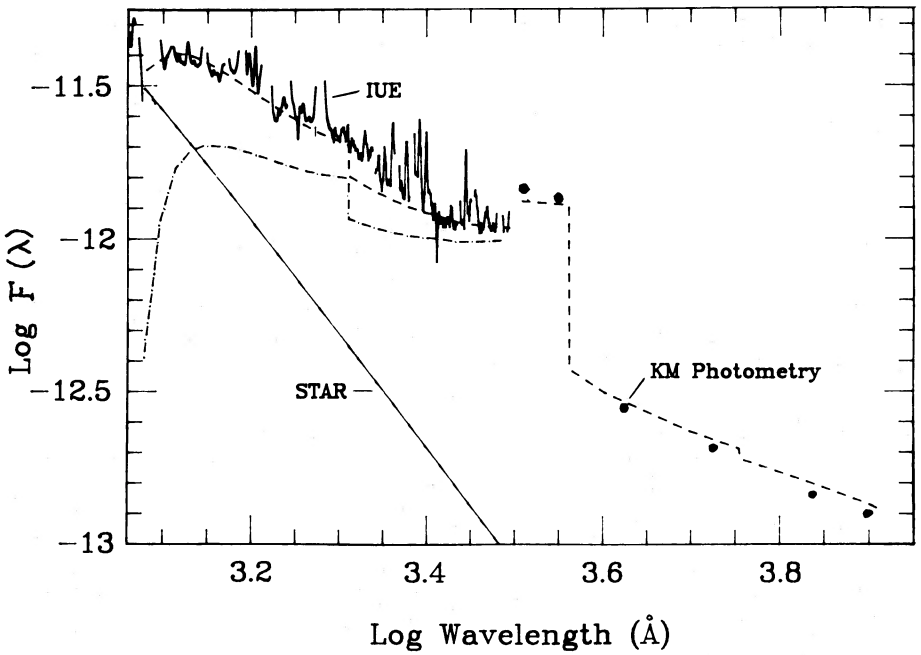

FIG. 9.—Decomposition of dereddened *IUE* and optical fluxes into contibutions from a hot star and from the nebular continuum of the model (*dash-dot line*). For log (λ) < 3.5, the dashed line shows the star plus 80% of the nebular continuum (to fit *IUE* data), while for log (λ) > 3.5 it shows the star plus 100% thereof (to fit the KM fluxes, denoted by dots).

TABLE 15

WIDTH OF *IUE* SPECTRUM (SWP 18028; LAP)

λ (Å)	FWHM	PSF	*F*(Star)/*F*(Neb.)
1909.....	5.10	2.85	...
1840.....	3.91	2.75	0.55
1690.....	3.70	2.53	0.66
1374.....	3.03	2.25	1.17
1308.....	2.29	2.25	1.70
1262.....	2.24	2.25	2.45

NOTE.—The measured full width at half-maximum (FWHM) and the camera's point spread function (PSF) are given in diagonal pixels. The ratio of stellar to nebular flux is taken from the decomposition shown in Fig. 9.

extended source (the nebular diameter out to 10% of central intensity is 17″), whereas the central star is a point source. This narrowing gives qualitative support to our decomposition of the total continuum.

The hot star continuum in Figure 9 is that of a non–LTE model atmosphere having $T_{\rm eff} = 140{,}000$ K, $\log g = 6.5$ and He/H = 0.10. It was one of a grid of non–LTE models calculated by us with the program of Mihalas and Auer (1975). The set of frequency points was extended to higher frequencies than in their work, up to a frequency $\nu = 7.8 \times 10^{16}$ s^{-1}, since the radiation field at depth extends to high frequencies in these hot models. The model flux is very similar to that of a blackbody in the near-ultraviolet, which corresponds to the Rayleigh-Jeans part of the spectrum. There is, hence little information about the stellar temperature from the continuum slope alone.

The measured stellar flux at 1300 Å is 2.4×10^{-12} ergs cm^{-2} s^{-1} Å^{-1} (although our models of § V were adjusted to have a slightly higher flux, measured from an earlier decomposition). The predicted (reddened) V-magnitude is 14.6, considerably fainter than some previous estimates (e.g., 10.84; Shao and Liller 1972), but only 0.3 mag fainter than the derived magnitude of KM. Knowledge of the stellar brightness now permits use of the Zanstra method. From the stellar flux at 1300 Å and the He II λ4686 flux we found the He II Zanstra temperature to be 126,000 K for a blackbody or 117,000 K for a non–LTE model atmosphere with He/H = 0.10 and $\log g = 6.0$. The H I Zanstra temperature is 90,000 K for a blackbody, which suggests that the nebula is more optically thin in H I than in He II. For the adopted distance of 1.5 kpc, the stellar luminosity is 4210 $L_\odot$ for the non–LTE 117,000 K model.

However, in § V we develop a model for NGC 3918 which includes a sector which is optically thin, even in He II. This allowed an upward correction of the He II Zanstra temperature to 140,000 K for a non–LTE model and enabled us to match the fluxes of high-excitation species such as Ne V, O V, and Mg V. The resulting luminosity is 6900 $L_\odot$. This is slightly higher than the value of 5900 $L_\odot$ derived by Martin (1981) from the optical fluxes of KM (the difference is just due to our higher reddening value).

For these adopted values of temperature and luminosity, the nucleus of NGC 3918 lies on the evolutionary track of a 0.64 $M_\odot$ core (Schonberner 1981), and the age since leaving the asymptotic giant branch is 3500 yr. This time scale is in fair agreement with the expansion age of the nebula: for O^{++} ions at the density maximum of our model (§ V), the expansion time is 2500 yr. This density maximum occurs at radius 0.05 pc, and the expansion velocity for [O III] lines is 20 km s^{-1} (Clegg, Sahu, and Walsh 1986). The calibration of Wood, Bessell, and Fox (1983) suggests that a 0.64 $M_\odot$ core mass comes from a star of initial mass in the range 1.3–1.7 $M_\odot$ (the uncertainty depending on the mass loss rate on the asymptotic giant branch). In our model the nebular mass is 0.26 $M_\odot$, and so a "missing" mass of 0.4–0.8 $M_\odot$ might reside in a faint outer "halo." The core mass and initial mass are uncertain because they depend on the adopted distance (through the stellar luminosity).

In summary, the central star of NGC 3918 has been detected indirectly through a decomposition of UV and optical continuum fluxes, and through the narrowing of the *IUE* spectrum near 1500 Å. The star was not seen directly, and no stellar features were detected on any of our spectra. The derreddened stellar flux at 1300 Å is 2.4×10^{-12} ergs cm^{-2} s^{-1} Å^{-1} and the predicted V-magnitude is 14.6. The corrected He II Zanstra temperature is 140,000 K and the luminosity 6900 $L_\odot$ for $d = 1.5$ kpc. The star is probably of spectral type sd0, with weak absorption features.

V. A MODEL FOR NGC 3918

a) The Computer Program

The modeling program was described by HSAL. The only significant changes since then are the inclusion of new atomic data. Dielectronic recombination coefficients for C, N, and O were taken from Nussbaumer and Storey (1983), and for all He ions plus Mg I, Si I, Si II, and Si III from Nussbaumer and Storey (1986). Charge transfer rates were as used by HSAL, except for new rates for N^{+4} (Feickert *et al.* 1984). The inverse ionization process $X^0 + H^+ \rightarrow X^+ + H^0$ was also introduced for the atoms Mg^0, S^0, and Si^0, with an assumed rate of 10^{-9} cm^3 s^{-1} (see Graedel, Langer, and Frerking 1982). Collision strengths were completely updated, from the compilation of Mendoza (1982) together with more recent data for Si III (Dufton, Keenan, and Kingston 1984), O IV (Hayes and Nussbaumer 1983), C II (Hayes and Nussbaumer 1984), and Mg I (H. E. Saraph, private communication).

For the Ne V fine structure lines from the ^3P ground state, we originally used the collision strengths of Aggarwal (1983). These values are ~10 times larger than those given by Osterbrock (1974) based on results from Saraph, Seaton, and Shemming (1970). However, we found a discrepancy of about a factor of 5 between the predicted and observed ratios of Ne V λ3426/14 μm if we used Aggarwal's data. The λ3426 line was observed at several positions in our own SAAO spectra (§ II*b*[ii]), and the value given in Table 14 is a mean. The 14 μm line is clearly detected in the *IRAS* low-resolution spectrometer spectrum of Pottasch *et al.* (1986). The *IRAS* band 1 ("12 μm") flux of 6.3 Jy is also impossible to reconcile with our λ3426 measurement, since the use of Aggarwal's data would imply a 14 μm line larger than the entire band 1 flux. Aggarwal's very detailed calculation for Ne V showed that there are large resonances at energies just above the thresholds for excitation of the fine-structure levels, and these dominate the thermal collision rate at 1 eV. Perhaps an even more refined calculation would give slightly lower energies for these resonances, in which case they would not contribute nearly so much to the thermally averaged rate. Note that Ne^{+4} would become an important coolant if the new rates are confirmed. The models presented here use the fine-structure collision strengths from Osterbrock (1974).

Pottasch *et al.* (1986) used the observed Ne V line flux ratio, 14 μm/λ3426, together with Aggarwal's data, to derive electron densities in several PNs. For NGC 3918 (and for several other objects) they obtained $N_e(Ne^{+4}) \approx 2 \times 10^5$ cm^{-3}, in disagreement with the results of Table 12. Pottasch *et al.* suggested that many PNs may have a high-density core, but we note that our [Ne IV] line ratios show no evidence for such a core. We suggest that the Ne V fine-structure collision strengths may be in error, and we note that, for Aggarwal's data, the critical density for the 14 μm line is 4.5×10^4 cm^{-3}. Analysis of an observed 14 μm line flux together with a very large value of the collision strength will often yield a value of N_e just above this density.

Treatment of the He^+ Lyα diffuse radiation was as described by HSAL, except that the fraction of recombinations released locally at a wavelength of 303 Å has been increased from 30% to 50%, since the escaping He^+ Lyα as well as the O III λ303.6 photons can suffer continuous absorption. The measured O III Bowen efficiency factor for NGC 3918, as defined by Saraph and Seaton (1980), is 0.58 ± 0.08. The models were iterated to convergence of the diffuse radiation field with the criterion that the largest temperature change between iterations be less than 5 K. It was found that convergence was slow (20 iterations needed) in the dense sector (see § V*b*) because this sector is optically thick in H and the ionizing radiation field is quite "hard" in that it extends to short wavelengths (especially since the NLTE model atmosphere has only H and He opacities and is rather transparent for wavelengths below 100 Å). Optically thin models converged in $\sim$5 iterations.

b) Methodology

We sought to construct a photoionization model for NGC 3918 which would reproduce the main observed characteristics of the nebula: the surface brightness distribution in Hβ light, the absolute Hβ and radio fluxes, and the relative strengths of important diagnostic lines. Our first approach was to seek a spherical model. The variation of hydrogen density with radius, $N_H(R)$, was derived from the average radial intensity profile in the Hβ map (shown in Fig. 4) using the method described in HSAL. This yielded the "shape" of the curve $N_H(R)$, which was then put on an absolute scale in cm^{-3} by matching the total Hβ flux for the adopted distance.

The observed intensities of low-excitation species such as O II, O I, and N II suggest that the nebula must be fairly optically thick in H I and therefore quite thick in He II. Hence, the He II Zanstra temperature was adopted for the stellar effective temperature (T = 117,000 K for a non–LTE model).

This approach did not succeed. Such a stellar model did not provide enough heating, and the nebular model was not able to reproduce the line strengths of high ionic stages such as O IV, Ne V, and O V. (The structure and density were heavily constrained by the observed Hβ map and observed line doublet ratios and could not be varied to produce these high-excitation lines). In addition, we knew from the two-dimensional spectral data and from the [O II] velocity data that the edge of the He II Strömgren sphere was not detected and that O^+ ions were mostly located at the front and rear of the object.

We therefore entertained conjecture of a composite model which was optically thick in some directions and optically thin in others, as seen from the central star. We considered the general case of a prolate spheroid (an ellipse rotated about its major axis) seen end-on, in which conical sectors at the front and rear may have density enhancements. The case (for a spherical version of this) is shown in Fig. 10. It was assumed that the radial density law followed the form

$$N_H(R) = N_0(R/R_1)^n \exp\left[-0.5(R/R_1)^2\right], \quad (1)$$

where N_0 is a normalization constant, and R_1 and n are parameters which were varied. This form, used by Harrington and Feibelman (1983), can represent both smooth, centrally condensed distributions (small n) as well as thin shells (large n). The maximum density occurs at $R = R_1 n^{1/2}$. The quantity R_1 is a scale length, and for our models it varies with angle θ (Fig. 10) so as to trace out an ellipse. The other parameters varied were Φ, the half-angle of the cones containing the dense sectors; f, the density enhancement factor in these sectors; and

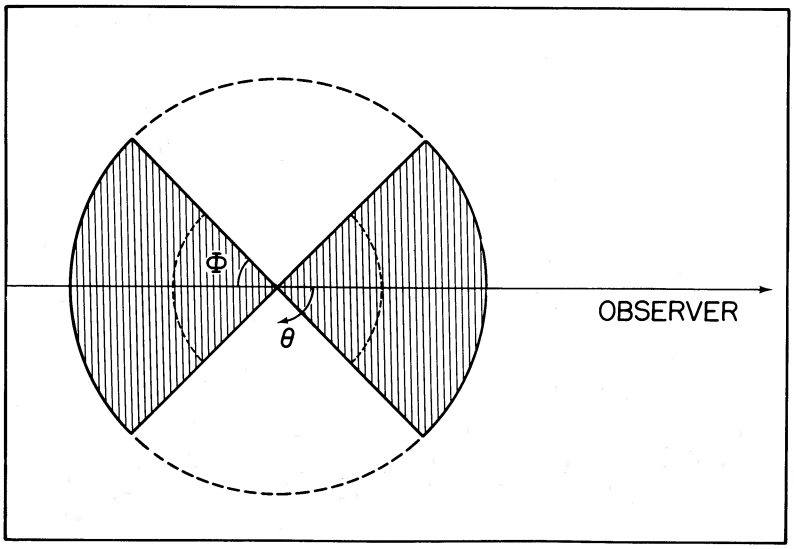

FIG. 10.—The final model. The structure shown is a solid of revolution about the line of sight. The cone angle $\Phi = 45°$. The dotted line shows the He II Strömgren radius, which coincides with the density maximum at a radius 0.05 pc. The densities in the front and rear cones are 3 times higher than those in the sides. The outer radius is 0.106 pc. The shape shown is idealized: the bicone may actually be tilted to the line of sight, as discussed in § II*d*.

the axial ratio of the spheroid. A computer program was written which calculated the radial intensity profile in Hβ light and the ratio of He II λ4686 to Hβ for this general configuration. The value of R_1 is essentially fixed by the low-intensity tail of the observed curve in Figure 4; Φ, n, f, and the axial ratio were varied.

c) *The Model*

After several models were calculated, all of which matched the Hβ map and the He II λ4686 flux, it was found that the best fit to the spectral data was obtained for the case with parameters $R_1 = 0.0333$ pc, $n = 2.3$, $f = 3$, $\Phi = 45°$, and an axial ratio of unity. The model is shown in Figure 10. No filling factor was required to match the observed density diagnostic ratios, and the density profile $N_H(R)$ can be calculated from equation (1) with the constant $N_0 = 2381$ cm^{-3} for the thin sector when R is in pc. The fit of the Hβ radial profile is shown in Figure 4, and the fit to the spectral line data and the absolute Hβ and radio fluxes is given in Table 16.

Three important points arise from the structure in Figure 10. (1) The low-density sector (which is like an equatorial "ring") is optically thin even in the He II continuum, with $\tau(228\ \text{Å}) = 1.1$. Correction of the He II Zanstra temperature for escaping He$^+$ continuum photons then allowed us to use a non–LTE model having $T_{\rm eff} = 140{,}000$ K for the central star. This produced larger fluxes from high-ionization stages such as Ne^{+4} and O^{+4}, in better agreement with observed fluxes. (2) A natural explanation is provided for the fact that the edge of the He II Strömgren sphere is not detected. Lines of sight at increasingly large impact parameters through the nebula (see Fig. 10) include an increasing contribution from the thin sector, where He is doubly ionized. The ratio of emissivities of He II λ4686 to Hβ is $\sim$1.1 in the thin sector, and so the observed ratio near the edge of the nebula need not be lower than that seen toward the center. (3) The low-excitation species such as O I, O II, and N II are preferentially located at the front and rear of the object, as demanded by the coudé spectrum of [O II] lines described in § II*c*.

The structure suggested here may also explain the faint outer "halo" detected in our slit spectra for the lines Hγ and He I λ5876 (see § II*b*[i]). Ionizing radiation leaks out of the "sides" of the nebula, which are quite optically thin. Any diffuse material outside the nebula can then easily be ionized. It is not known if the faint outer extensions seen in the Hγ and He I lines represent a low-density outer nebular shell or ionized diffuse interstellar material. We calculated the rms electron density needed to yield the observed surface brightness in the Hγ line (§ II*b*[i]) at large offsets from the nebular center. At radii of 17″ and 21″, the rms densities are 120 and 40 cm^{-3} respectively. If such a "halo" is spherically symmetric, the mass implied is only 0.01 $M_\odot$.

Table 16 shows the contributions to the line fluxes from the individual sectors. Since the cone angle $\Phi = 45°$, the thin "equatorial" region occupies 71% of the volume, but because of its low density it only contributes 19.6% of the total Hβ flux. The observed fluxes listed in the table are for the whole object. The observed and predicted fluxes in the infrared region are shown separately, in Table 17, because there are special problems with the measurement and calibration of IR fluxes. The agreement of the fine-structure line fluxes from the *IRAS* spectrometer, in the 9–22 μm region, is not good. Predicted fluxes for the strongest unobserved lines in the IR are given, as a guide for future observations.

The mean energy per photoionization from the model atmosphere is 19.8 eV for H and 29.9 eV for He$^+$ in the thick sector. Corresponding values for a 140,000 K blackbody are 17.1 and

TABLE 16

OBSERVED AND MODEL FLUXES[a] FROM IMPORTANT LINES

Ion	λ (Å)	Model			Observed (Dereddened)
		Thin	Thick	Total	
H I	4861	0.45	1.86	2.32	$2.5 \pm 0.2 \times 10^{-10}$
(Radio)	(5 GHz)	0.71	0.23	0.94	(0.86 ± 0.06 Jy)
He II	4686	22	26	48	45
He I	5876	0.06	7.7	7.8	9.5
C IV	4658	0.24	0.16	0.40	0.42
C IV	1550	659	779	1439[b]	512
C III	2297	1.0	4.9	5.9	5:
C III	4648	0.10	0.42	0.52	0.47
C III	1908	58.7	577	637	540
C II	4267	0.006	0.32	0.32	0.43
C II	2236	0.72	81	82	35
N V	1240	47	19	66[b]	46
N IV	1486	31	26	57	50
N III	1751	4.6	25	29	29
N II	6584	0.2	73	73	64
O IV	1342	1.0	0.6	1.6	2:
O IV	1402	28	16	43	40
O III	5007	63	1539	1602	1560
O III	4363	1.4	18.9	20	20
O II	3727	0.2	89	89	65
O I	6300	0.0	0.56	0.56	4
O III	5592	0.04	0.07	0.11	0.07
Ne V	3426	70	40	110	80
Ne IV	2423	50	52	102	132
Ne III	3868	3	172	175	120
Si IV	1399	2.8	5.4	8.2[b]	9
Si III	1887	1.2	12.5	13.7	8
S IV	10 μm	24	210	234	64
S III	6312	0.05	3.4	3.4	3
S II	4070	0.00	2.8	2.8	2.5
Mg V	2783	3.2	2.6	5.8	5.6
Mg II	2800	0.01	43	43[b]	≤ 1
Mg I	4565	0.00	0.28	0.28	0.41

[a] Relative to the total Hβ flux, 2.5×10^{-10} ergs cm^{-2} s^{-1}, and on the scale $I(\text{H}\beta) = 100$. The Hβ and radio fluxes are absolute. The contributions from each sector are shown.

[b] Attenuated by dust.

TABLE 17

INFRARED LINE FLUXES

λ (μm)	Ion	Model			Observed[a]
		Thin	Thick	Total	
4.5.....	Mg IV	0.96	4.4	5.4	...
5.6.....	Mg V	4.9	5.4	10.3	...
7.6.....	Ne VI	11.	4.9	15.8	...
10.5.....	S IV	24.	210.	234	64
12.8.....	Ne II	0	0.77	0.77	12:
14.3.....	Ne V	18	13	31	48
15.6.....	Ne III	1.3	167	168	88
18.7.....	S III	0.31	38	38	12:
24.3.....	Ne V	30	19	49	...
25.9.....	O IV	274	177	451	...
33.6.....	S III	0.2	15.6	16	...
36.0.....	Ne III	0.11	13.	13	...
51.8.....	O III	4.0	94	98	...
57.3.....	N III	1.0	12	13	...
88.4.....	O III	1.3	17	19	...

[a] Pottasch *et al.* 1986.

TABLE 18

FRACTIONAL IONIC ABUNDANCES

	Ion[a]						
Element	I	II	III	IV	V	VI	VII
H	0.92(−2)	0.991	...	...	...	...	...
	0.53(−3)	0.999	...	...	...	...	...
He	0.20(−2)	0.683	0.315	...	...	...	...
	0.73(−5)	0.026	0.974	...	...	...	...
C	0.19(−3)	0.066	0.512	0.289	0.134	...	...
	0.27(−6)	0.60(−3)	0.044	0.244	0.712	...	...
N	0.63(−3)	0.071	0.511	0.333	0.059	0.025	...
	0.10(−6)	0.36(−3)	0.074	0.405	0.324	0.196	...
O	0.14(−2)	0.053	0.708	0.174	0.047	0.014	0.24(−2)
	0.36(−7)	0.15(−3)	0.057	0.517	0.300	0.107	0.018
Ne	0.73(−5)	0.78(−2)	0.682	0.183	0.111	0.015	0.51(−3)
	0.18(−8)	0.24(−4)	0.019	0.325	0.541	0.112	0.37(−2)
S	0.75(−5)	0.024	0.301	0.483	0.095	0.072	0.024
	0.24(−8)	0.27(−4)	0.76(−2)	0.171	0.205	0.426	0.191
Si	0.30(−3)	0.285	0.189	0.213	0.251	0.060	...
	0.12(−5)	0.77(−3)	0.016	0.076	0.578	0.328	...
Mg	0.40(−3)	0.058	0.566	0.142	0.164	0.069	...
	0.86(−7)	0.11(−4)	0.48(−2)	0.105	0.499	0.391	...

[a] For each ion the upper entry is for the dense sector, the lower for the thin. Parentheses enclose powers of factor 10.

17.0 eV, so the model provides significantly more heating. Torres-Peimbert, Pena, and Daltabuit (1981) presented a model for this PN with a star represented by a blackbody at 150,000 K, a value similar to our adopted $T_{\rm eff}$. The ratio of fluxes in collisionally excited cooling lines to the Hβ flux for the whole nebula is 71 in the model, of which 3.3 arises from (unobservable) excitation of neutral H. The difference, 68, is in agreement with our early empirical value of 67, which consisted of a contribution of 50.0 from directly observed lines plus a value of 17 from predictions of unobserved lines, mostly in the IR. Thus 75% of the cooling flux is directly observed. The optical depths at threshold in our model are τ(H) = 49.2, τ(He) = 1.2, and $\tau(He^+)$ = 80.5 for the dense sector; and τ(H) = 0.89, τ(He) = 0.001, and $\tau(He^+)$ = 1.1 for the thin sector. The total mass of the nebula is 0.26 $M_\odot$.

The strengths of low-ionization lines are very sensitive to the optical depth of the dense sector. Models constructed with a slightly less luminous central star, or a slightly higher density, show significantly stronger lines of [O I], [O II], and [N II], with the [O I] λ6300 line increasing more dramatically than [O II] λ3727 or [N II] λ6584. In a model with an 8% less luminous star or a 4% higher density, τ(H) would increase to 300 and produce the observed flux in [O I] λ6300, but the [O II] and [N II] lines would then be 50% stronger. We chose to match the [O II] and [N II] lines, as they represent more of the nebular material, with the result that the [O I] line is too weak by a factor of 7. It seems plausible that the thick sectors are not completely uniform, and that an average over different radial density laws would result in the observed [O I]/[O II] intensity ratio.

This is a composite model, and the fluxes from each sector are weighted by that sector's volume to form the total flux relative to the total Hβ flux from the nebula. The contribution from each sector is listed in Tables 16 and 17. In Tables 18 and 19, we present the fractional ionic abundances and the temperatures weighted by each ionic species, for each sector. These quantities are defined as in Tables 15 and 17 of HSAL. In the thin sector the minimum electron temperature is 15,700 K, while in the thick sector the minimum value is 11,500 K at R = 0.0615 pc. The fractional ionic abundances can be used in conjunction with the respective temperature to make reason-

TABLE 19

MEAN TEMPERATURES (K) WEIGHTED BY IONIC SPECIES

	Ion[a]						
Element	I	II	III	IV	V	VI	VII
H	12,100	12,920	...	...	...	...	...
	16,330	16,770	...	...	...	...	...
He	12,030	12,070	14,750	...	...	...	...
	16,100	16,270	16,780	...	...	...	...
C	12,070	12,070	12,200	13,050	15,760	...	...
	16,030	16,060	16,160	16,330	16,950	...	...
N	12,060	12,070	12,280	13,220	15,620	17,610	...
	16,000	16,050	16,150	16,350	16,760	17,870	...
O	12,060	12,060	12,210	14,690	16,030	17,620	21,040
	15,950	16,020	16,130	16,400	16,900	17,830	20,730
Ne	12,030	12,010	12,070	14,130	15,450	17,550	22,610
	15,940	16,000	16,090	16,320	16,770	17,980	22,290
S	12,090	12,070	12,090	12,600	13,970	15,710	17,640
	15,960	15,980	16,060	16,170	16,380	16,730	17,830
Si	12,090	12,040	12,170	12,570	14,040	15,940	...
	16,030	16,030	16,100	16,210	16,540	17,330	...
Mg	12,060	12,000	11,990	13,480	14,750	16,180	...
	15,910	15,940	16,010	16,180	16,510	17,250	...

[a] For each ion the upper entry refers to the dense sector, the lower to the thin.

ably accurate estimates of the intensities of any emission lines of interest.

Each sector is modeled as if it were a complete sphere. Therefore, the diffuse radiation field within the model is not self-consistent, especially near the sector boundaries. We do not expect that the effects of this inconsistency will be large. Another model might be conjectured, in which many thick and thin zones are interleaved; apart from the effects of the diffuse radiation field, the total fluxes of such a model would be the same as those presented here. However, we adopt the geometry of Figure 10 because of the [O II] coudé spectrum. Also, it has not escaped our attention that this geometry is known to occur in another planetary, NGC 6853, for which a similar structure is seen side-on rather than end-on.

The effects of dust grains are not included in this model. In an accompanying paper, Harrington, Monk, and Clegg (1987) present a dust model for NGC 3918 which includes the effects of the dust on the ionization model. Aside from the reduction of the intensities of resonance lines, the dust model is nearly identical to that presented here.

During the modeling, elemental abundances and the stellar luminosity were adjusted slightly from the empirical values found in § III, in order to provide the best match to observed line fluxes. The adjustments are mostly due to differences between estimated and model electron temperatures. Adopted abundances for the eight elements included are given in Table 20. The nebula is C-rich, with C/O = 1.6 (in agreement with the result of Torres-Peimbert, Pena, and Daltabuit 1981). The central star parameters $T_{\rm eff} = 140{,}000$ K, $L = 6900\ L_\odot$ imply $R_* = 0.142\ R_\odot$ and a flux at 1300 Å, $F = 2.9 \times 10^{-13}$ ergs cm^{-2} s^{-1} Å^{-1}, slightly higher than the value derived in § III*d* but within the error of measurement.

We discuss briefly the uniqueness and the errors in our model. Is the derived structure unique? Probably, other combinations of geometry and density law can match the observations. But since any plausible model must have most of the [O II] emission at the front and rear preferentially and must have some optically thin zones extending right out to the nebular edge, other models may not look very different from ours. The bicone of Figure 10 is shown end-on but in fact may be slightly tilted, as we noted in § II*d*. Errors in abundances vary greatly by element. We estimate that the helium abundance is accurate to 10%; CNO and Ne to 40%; Mg, Si, S, and Ar only to 60%; and Fe only to about a factor of 2. An example of the difference between model and empirical abundances is seen in the result for carbon: we found C/H = 1.0×10^{-3} empirically (but using model predictions for the electron temperatures of each ion), while the best 'model' C/H ratio matching many lines was 8.0×10^{-4}. We suggest that the best procedure for deriving PN abundances is empirical analysis of observed line fluxes using model predictions for unmeasured ionic electron temperatures and model corrections for unseen ionization stages.

TABLE 20

FINAL ABUNDANCES FOR NGC 3918 RELATIVE TO H

Element	Abundance	Method[a]
He	0.107	E
C	8.0×10^{-4}	M
N	1.5×10^{-4}	M
O	5.0×10^{-4}	M
Ne	1.2×10^{-4}	M
Mg	1.4×10^{-5}	M
Si	1.0×10^{-5}	M
S	1.6×10^{-5}	M
Ar	2.0×10^{-6}	E
Fe	3.7×10^{-7}	E

[a] E, based on empirical analysis; M, from final photoionization model.

d) Resonance Lines

The observed resonance lines Mg II λ2800, C II λ1335, Si IV λ1397, C IV λ1550, and N V λ1240 may be weakened by dust absorption. Indeed, the observed attenuation of 1550 Å in some nebulae (e.g., Harrington, Lutz, and Seaton 1981) and the observed thermal IR emission (e.g., Cohen, Harrington, and Hess 1984) both provide the evidence that dust grains are present even in the inner regions of the ionized gas. The optical depths of these lines are respectively 0.07, 58, 123, 8430, and 1720 in the thin sector; and 1430, 24,700, 1190, 36,600, and 1890 in the thick sector. In our modeling we did not attempt to match the exact values of the observed fluxes of these lines.

The attenuation of 1550 Å is indicated by the ratios of the recombination lines C III λλ2297, 4648 to C IV λ1550. Without allowance for attenuation, these line ratios would imply $T_e(C^{+3}) = 12{,}300$ K, lower than the measured temperature from Ar V, Ne IV, Ne V, and even O III (Table 12). Another indication is the good fit of the model prediction to the observed N IV] λ1486 line; the ionization potentials of N^{++} and C^{++} are similar. Dust absorption of the Mg II, C II, Si IV, and N V lines is harder to demonstrate: the predicted N V line is stronger than observed, but the Si IV lines are not. We found weak evidence for attenuation of 1240 Å from a comparison of its flux with that of N IV λ1718 (measured off the image SWP 18029; see also Table 13). A similar result was given by Pena and Torres-Peimbert (1985). Comparison of N IV λ1406 with 1240 Å (Tables 13 and 14) also suggests little attenuation of the N V resonance line. The Si IV doublet is weak and difficult to measure, and it is not as optically thick as the other lines. The C II λ1335 and Mg II λ2800 lines are not detected in our spectra, but this is inconclusive because they both suffer from interstellar absorption, as discussed in the next section.

e) The Magnesium Lines

We set the Mg abundance of the model at Mg/H = 1.4×10^{-5} to match the observed Mg V λ2783 flux. The model prediction for the Mg I] λλ4562, 4571 flux is then close to the observed value. The strength of Mg I] is not simply related to the strength of [O I] λ6300 as discussed in § V*c*, because the distribution of Mg^0 atoms within the model does not show a concentration to the edge like O^0 atoms, but rather they are distributed like the O^+ ions. The concentration of Mg^0 in the model is in fact inversely proportional to the rate of the $Mg^0 + H^+ \rightarrow Mg^+ + H^0$ process. Olson and Liu (1979) calculated this rate at energies between 50 eV and 1 keV. Crude extrapolation of their cross sections to 1 eV would suggest a rate on the order of 10^{-9} cm^3 s^{-1} at 10^4 K; but a calculation or measurement at low energies is needed. We have used 10^{-9} cm^3 s^{-1} as a crude estimate. The agreement of predicted and observed Mg I] fluxes is somewhat fortuitous, given the uncertainty in the charge transfer rate. But the process is of extreme importance for the Mg I] lines: if the rate is set to zero, the line would be 40 times stronger.

Our adopted Mg abundance results in a predicted Mg II λ2800 line that is too strong by a factor of 40 when compared

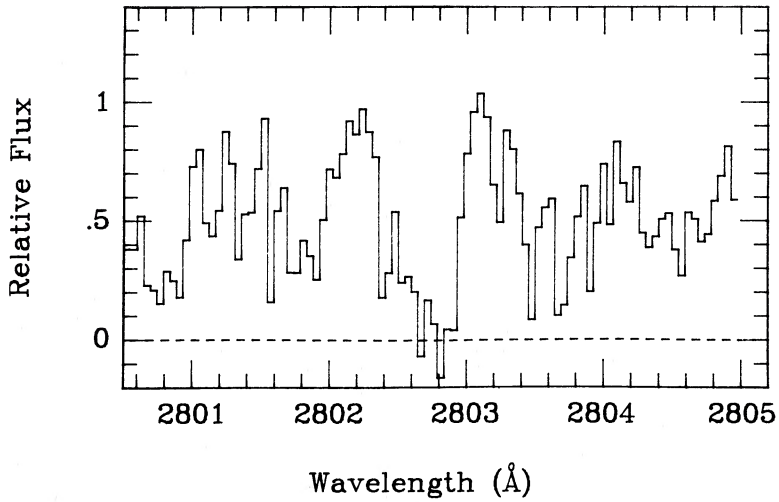

FIG. 11.—Part of the high-dispersion *IUE* image LWP 2407 (order 82). The Mg II λ2802.7 line suffers absorption (FWHM 65 km s^{-1}), but the outermost parts of the emission line wings can be seen.

to the observed upper limit. Internal absorption by dust would be expected to reduce the intensity of the line by a factor of 1.5–2.0 (Harrington, Monk, and Clegg 1987), which does little to mitigate the disagreement. However, examination of the high-resolution image LWP 2407 (Fig. 11) shows that Mg II λ2802.7 is cut by an absorption feature 65 km s^{-1} in width, fully as wide as the expected nebular emission lines. (The resolution of the *IUE* LWP camera is ~25 km s^{-1} for a point source and ~100 km s^{-1} for a very extended source; the absorption line width measured here probably reflects the instrumental resolution for this extended nebula). The Mg II absorption feature appears to be centered at the nebular systemic velocity; its wavelength was measured relative to nebular emission features in nearby orders of the LWP echelle spectrum, and no velocity shift was found within an uncertainty of 5 km s^{-1}. This result differs from that for the Na I absorption, which is centered on +19 km s^{-1} in the nebular frame. The neutral and ionized absorbers are probably located in different clouds. (A broad absorption feature was also seen at the position of the Mg I resonance line at 2852 Å, but it was difficult to measure because of the weakness of the continuum). In any case, the λ2800 line can provide no information about the nebular abundance of Mg^+ ions.

The Mg II absorption is surely interstellar in origin and is most likely related to the absence of C II λ1335 in *IUE* spectra. The upper limit for 1335 Å, derived from the low-resolution image SWP 18029, is 3×10^{-12} ergs cm^{-2} s^{-1}. After taking into account the expected internal dust extinction of 50% and the fact that the model overestimates the C^+ abundance by a factor of 2 (as judged from the strength of C II λ2326), we predict the λ1335 line to have a flux of 8×10^{-12} ergs cm^{-2} s^{-1}. Unfortunately, no continuum is seen in the high-resolution SWP images, so our hypothesis of absorption cannot be directly verified.

The C II discrepancy in NGC 3918 is similar to, but less extreme than, the case of NGC 40, for which Clegg *et al.* (1983) found the line to be absent with an upper limit a factor of 12 below the predicted value. In the PN IC 418, Clavel, Flower, and Seaton (1981) found both absorption and redshifted emission in this line. IC 418 has a high velocity of $V(LSR) = +43$ km s^{-1}, so that the nebular emission mostly escapes the interstellar absorption.

The column density of H toward NGC 3918 is 2×10^{21} cm^{-2} (§ III*a*). If we assume that the Mg in the interstellar medium (ISM) is depleted by 0.8 dex and that gaseous Mg is in the form Mg^+, the column density of this ion would be ~10^{16} cm^{-2}. A cloud with an internal turbulent velocity 8 km s^{-1} and a column of only 10^{15} cm^{-2} would produce a line with optical depth of 700. Thus there should be plenty of material to produce the required absorption; the question is only whether the various clouds along the line of sight span a sufficient range in velocity to completely extinguish a line of full width ~50 km s^{-1}. From the evidence of Figure 11, toward NGC 3918 they apparently do just cover this velocity range (the extreme wings of the line are seen in emission in the figure). The radial velocity of NGC 3918 is $V(LSR) = -24$ km s^{-1} (Schneider *et al.* 1983); it is at Galactic longitude 194°, so that differential Galactic rotation will give the intervening ISM a negative velocity as well.

To confirm that interstellar Mg II lines can indeed achieve widths of 30–50 km s^{-1}, we examined line profiles in reddened hot stars from Pettini (1976) and from *IUE* high-resolution spectra taken by Dr. W. B. Somerville. We measured full widths at 80% depth of Mg II λλ2795.7, 2802.7 and Mg I λ2852.1. For Mg II, Pettini showed that two stars with $E(B-V) = 0.10$ had widths of 19 and 51 km s^{-1}. The *IUE* spectra of stars having $E(B-V)$ between 0.3 and 0.7 gave widths between 27 and 94 km s^{-1}. Mg I widths were generally ~60% of Mg II widths. The Mg II lines are evidently so strong that many interstellar clouds contribute even to the deepest part of the absorption profile. This result will surely also apply to the C II λ1335 lines. In both cases nebular emission lines can be completely extinguished.

The weakness of the observed Mg II doublet in PNs when compared to model predictions has been noted in many cases, first by Pequignot and Stasinska (1980) in NGC 7027. They suggested that Mg might be depleted by grain formation in the outer parts of the nebula but not in the inner regions where Mg^{+4} is found. Harrington and Marionni (1982) found the same effect in IC 2165 and NGC 2440 and also interpreted the weak Mg II line as sign of depletion, as did HSAL for NGC 7662 and Flower and Penn (1981) for NGC 6572. However, there appears to be a correlation of Mg II line strength with radial velocity, which again suggests that interstellar absorp-

tion is important. We give LSR radial velocities in km s^{-1}. Those PNs which show little or no Mg II tend to have low velocities (NGC 6572, $V = +9.6$; NGC 7662, $V = -4.7$; NGC 40, $V = -11.6$), while the few PNs with strong Mg II have high velocities: IC 418, $V = +43.4$, in which $I(2800)/H\beta = 0.23$ (Harrington *et al.* 1980); and NGC 6741, for which $V = +58$ and $I(2800)/H\beta = 0.6$ (Aller, Keyes, and Czyzak 1985). We therefore caution against the use of the Mg II line to infer ionic abundances unless the nebula is of a very high velocity, or high-resolution spectra exist which demonstrate the absence of interstellar absorption.

f) Depletion of Elements

From the final abundances given in Table 20, we found that three elements are significantly depleted relative to the solar value: Fe by a factor of 100, Si by a factor of 4, and Mg by a factor of 3. S is not depleted. Here we adopted solar abundances 4×10^{-5} for Fe, Mg and Si; and 1.6×10^{-5} for S. The Fe abundance is based on the derived Fe^{+5} and Fe^{+6} fractions with an ionization correction factor of 5.5 and is probably uncertain to a factor of 2–3.

Savage and Mathis (1979) reviewed heavy element depletions in diffuse interstellar clouds. Toward ζ Oph, Mg, Si, and Fe are depleted by 1.7 dex; toward ζ Pup, Mg and Si are only reduced by 0.8 dex, while Fe is deficient by 1.2 dex. In general, S is little depleted (up to 0.2 dex) in diffuse clouds. These results are only broadly similar to the results for PNs: S is little depleted, while Fe may be down by 0.4–2.0 dex (Shields 1978). Si can be reduced by 1 dex (Harrington and Marionni 1982). The depletion pattern for NGC 3918 very approximately resembles that of ζ Pup. Its reduction of iron equals the maximum of 2 dex found by Shields (1978) (for NGC 6886).

VI. CONCLUSIONS AND IMPLICATIONS

We have presented a model for NGC 3918 which met certain criteria in matching these quantities: the $H\beta$ surface brightness map, the absolute $H\beta$ and radio fluxes, the stellar continuum at 1300 Å, density diagnostic ratios, and a large amount of spectral information. Our goal was to make a highly detailed model for a "reference" PN which can be used in the future to study physical processes. For example, in accompanying papers, processes involving dust and charge transfer between Ne^{+3} and H are modeled in this object. In the current modeling we introduced charge exchange reactions between Mg^0, Si^0, and S^0 with protons (since these neutral atoms have ionization potentials less than that of H) and obtained better agreement with observed Mg I] line strengths.

There are two important consequences of our adopted model, which "leaks" a considerable number of ionizing photons into the interstellar medium. First, even for PNs which are thought to be optically thick (on the basis of strong [O II], [N II], or [O I] lines), the stellar He II Zanstra temperature may need upward correction. Nebulae may be optically thick in some directions and optically thin in others. If the model of Figure 10 were seen side-on, we would predict that the hot central star should be seen as a source of soft X-rays, in the absence of interstellar absorption. In fact, NGC 3918 is too highly reddened for the X-rays to be detected, but such a situation may actually be realized for a nebula with a similar structure: the "Dumbbell" nebula NGC 6853 is seen side-on and was detected in the X-ray region by the *Einstein* satellite (Vedder and Clark 1982). Thus while NGC 6853 shows strong lines of [O II] and [O I], it may be optically thin along the line of sight toward its central star. A cautionary note is therefore sounded about the use of Zanstra temperatures. The effect described here is largest for hot central stars ($T > 100{,}000$ K): for cooler stars, correction of the Zanstra temperature (even by a factor of 2 in the number of He II continuum photons) results in only a small change in the derived value of T_Z.

A brief comparison with NGC 6853 is warranted here. Bohlin, Harrington, and Stecher (1982) derived central star properties $T_{\rm eff} = 144{,}000$ K and $L = 200\ L_\odot$ for a distance of 260 pc. The radius of its "thick sector" is 0.19 pc. While its star temperature is similar to that of NGC 3918, the larger radius and lower star luminosity both attest to its more advanced age.

Second, PNs such as NGC 3918 provide a large flux of ionizing photons for the ISM and the Galactic Halo. The number of escaping photons is 9.4×10^{46} s^{-1} between 13.6 and 54.2 eV, and 1.7×10^{47} s^{-1} at energies above 54.2 eV. While there exists a class of large, old, low-density planetaries which are optically thin and have hot central stars (Kaler 1981), NGC 3918 has a much higher luminosity (6900 $L_\odot$) than these objects and provides a greater ionizing flux. We note that the leaked stellar photons with more than 77 eV can produce N^{+4} ions, which are seen in a few parts of the Galactic Halo (Pettini and West 1982) and along lines of sight toward distant stars at low Galactic latitude (Savage and Massa 1985).

We thank the UK SERC's Panel for Allocation of Telescope Time for observing time at the SAAO and AAT, and the Director of the Anglo-Australian Observatory for Director's time on the AAT. We thank Drs. Peter Wood and Mike Bessell for the [O II] coudé spectrum, and Drs. K. Reay and S. P. Worswick for permission to trace their electronographic plates. J. R. W. thanks the SAAO staff for assistance with observations made there in 1982. Some of the *IUE* spectra were taken by Prof. M. J. Seaton. Drs. P. J. Storey and D. R. Flower and Prof. Seaton gave useful comments on atomic data, and we thank Dr. H. Saraph for communicating her Mg I collision strengths. Dr. W. B. Somerville kindly gave us access to his *IUE* spectra.

Our collaborative computational work was assisted by SERC's CCP7. R. E. S. C. was supported by SERC, and J. P. H. by the NSF, grant AST-84-00994.

REFERENCES

Acker, A. 1976, *Pub. Obs. Astr. Strasbourg*, Vol. **4**, pt. 1.
Aggarwal, K. M. 1983, *J. Phys. B.*, **16**, 2405.
Aller, L. H., Keyes, C. D., and Czyzak, S. J. 1985, *Ap. J.*, **296**, 492.
Barker, T. 1984, *Ap. J.*, **284**, 589.
———. 1985, *Ap. J.*, **294**, 193.
Beck, S. C., Lacey, J. H., Townes, C. H., Aller, L. H., Geballe, T. R., and Baas, F. 1981, *Ap. J.*, **249**, 592.
Bohlin, R. C., Harrington, J. P., and Stecher, T. P. 1982, *Ap. J.*, **252**, 635.
Bohlin, R. C., Savage, B. D., and Drake, J. F. 1978, *Ap. J.*, **224**, 132.
Brocklehurst, M. 1971, *M.N.R.A.S.*, **153**, 471.
Carrasco, L., Serrano, A., and Costero, R. 1983, *Rev. Mexicana Astr. Ap.*, **8**, 187.
Clavel, J., Flower, D. R., and Seaton, M. J. 1981, *M.N.R.A.S.*, **197**, 301.
Clegg, R. E. S., Harrington, J. P., and Barlow, M. J. 1984, in *Proc. 4th ESA IUE Conf.* (Noordwijk: ESA SP-128), p. 337.
Clegg, R. E. S., Sahu, K. C., and Walsh, J. R. 1986, in preparation.
Clegg, R. E. S., Seaton, M. J., Peimbert, M., and Torres-Peimbert, S. 1983, *M.N.R.A.S.*, **205**, 417.
Clegg, R. E. S., and Walsh, J. R. 1985, *M.N.R.A.S.*, **215**, 323.
Cohen, M., Harrington, J. P., and Hess, R. 1984, *Ap. J.*, **283**, 687.
Coleman, C. I., Reay, N. K., and Worswick, S. P. 1975, *M.N.R.A.S.*, **171**, 415.
Dufton, P. L., Keenan, F. P., and Kingston, A. E. 1984, *M.N.R.A.S.*, **209**, 1P.
Feickert, C. A., Blint, R. J., Surratt, G. T., and Watson, W. D. 1984, *Ap. J.*, **286**, 371.

Flower, D. R., and Penn, C. J. 1981, *M.N.R.A.S.*, **194**, 13P.
French, H. B. 1983, *Ap. J.*, **273**, 214.
Garstang, R. H. 1957, *M.N.R.A.S.*, **117**, 329.
Garstang, R. H., Robb, W. D., and Rountree, S. P. 1978, *Ap. J.*, **222**, 384.
Graedel, T. E., Langer, W. D., and Frerking, M. A. 1982, *Ap. J. Suppl.*, **48**, 321.
Grandi, S. A. 1976, *Ap. J.*, **206**, 658.
Harrington, J. P., Clegg, R. E. S., and Monk, D. J. 1984, *Bull. AAS*, **16**, 976.
Harrington, J. P., and Feibelman, W. A. 1983, *Ap. J.*, **265**, 258.
Harrington, J. P., Lutz, J. H., and Seaton, M. J. 1981, *M.N.R.A.S.*, **195**, 21P.
Harrington, J. P., Lutz, J. H., Seaton, M. J., and Stickland, D. J. 1980, *M.N.R.A.S.*, **191**, 13.
Harrington, J. P., and Marionni, P. 1982, in *The Universe at Ultraviolet Wavelengths*, ed. R. D. Chapman (NASA CP-2171), p. 623.
Harrington, J. P., Monk, D. J., and Clegg, R. E. S. 1987, *Ap. J.*, submitted.
Harrington, J. P., Seaton, M. J., Adams, S., and Lutz, J. H. 1982, *M.N.R.A.S.*, **199**, 517 (HSAL).
Hayes, M. A., and Nussbaumer, H. 1983, *Astr. Ap.*, **124**, 279.
———. 1984, *Astr. Ap.*, **134**, 193.
Hobbs, L. M. 1974, *Ap. J.*, **191**, 381.
Kaler, J. B. 1981, *Ap. J.* (*Letters*), **250**, L31.
———. 1982, in *IAU Symposium 103, Planetary Nebulae*, ed. D. R. Flower (Dordrecht: Reidel), p. 245.
Kaler, J. B., Aller, L. H., Czyzak, S., and Epps, H. 1976, *Ap. J. Suppl.*, **31**, 163.
Kohoutek, L., and Martin, W. 1981, *Astr. Ap. Suppl.*, **44**, 325.
Kupferman, P. N. 1983, *Ap. J.*, **266**, 689.
Martin, W. 1981, *Astr. Ap.*, **98**, 328.
Mendoza, C. 1982, in *IAU Symposium 103, Planetary Nebulae*, ed. D. R. Flower (Dordrecht: Reidel), p. 143.
Mihalas, D., and Auer, L. H. 1975, NCAR-TN/STR-104.
Milne, D. K., and Aller, L. H. 1975, *Astr. Ap.*, **38**, 183.
Milne, D. K., and Webster, B. C. 1979, *Astr. Ap. Suppl.*, **36**, 169.
Nussbaumer, H., and Storey, P. J. 1978, *Astr. Ap.*, **70**, 37.
———. 1982, *Astr. Ap.*, **113**, 21.
———. 1983, *Astr. Ap.*, **126**, 75.
———. 1984, *Astr. Ap. Suppl.*, **56**, 293.
———. 1986, preprint.
Oke, J. B. 1974, *Ap. J. Suppl.*, **27**, 21.
Olson, R. E., and Liu, B. 1979, *Phys. Rev. A*, **20**, 1366.
Osterbrock, D. E. 1974, *Astrophysics of Gaseous Nebulae* (San Francisco: Freeman).
Pena, M., and Torres-Peimbert, S. 1983, *Rev. Mexicana Astr. Ap.*, **5**, 313.
———. 1985, *Rev. Mexicana Astr. Ap.*, **11**, 35.
Pengelly, R. M. 1963, Ph.D. thesis, University College London.
Pequignot, D., and Stasinska, G. 1980, *Astr. Ap.*, **81**, 121.
Pettini, M. 1976, Ph.D. thesis, University of London.
Pettini, M., and West, K. A. 1982, *Ap. J.*, **260**, 561.
Pottasch, S. R. 1982, in *IAU Symposium 103, Planetary Nebula*, ed. D. R. Flower (Dordrecht: Reidel), p. 391.
Pottasch, S. R., Preite-Martinez, A., Olnon, F. M., Jing-Er, M., and Kingma, S. 1986, *Astr. Ap.*, **161**, 363.
Sabbadin, F. 1984, *M.N.R.A.S.*, **210**, 341.
Saraph, H. E., and Seaton, M. J. 1970, *M.N.R.A.S.*, **148**, 367.
———. 1980, *M.N.R.A.S.*, **193**, 617.
Saraph, H. E., Seaton, M. J., and Shemming, J. 1970, *Phil. Trans. Roy. Soc. London*, **A264**, 77.
Savage, B. D., and Massa, D. 1985, *Ap. J.* (*Letters*), **295**, L9.
Savage, B. D., and Mathis, J. S. 1979, *Ann. Rev. Astr. Ap.*, **17**, 73.
Schonberner, D. 1981, *Astr. Ap.*, **103**, 119.
Seaton, M. J. 1977, in *IAU Symposium 76, Planetary Nebulae Observations and Theory*, ed. Y. Terzian (Dordrecht: Reidel), p. 131.
———. 1978, *M.N.R.A.S.*, **185**, 5P.
———. 1979, *M.N.R.A.S.*, **187**, 73P.
Seaton, M. J., and Storey, P. J. 1976, in *Atomic Physics and Applications*, ed. P. G. Burke and B. L. Moisewitch (Amsterdam: North Holland).
Schneider, S. E., Terzian, Y., Purgathofer, A., and Perinotto, M. 1983, *Ap. J. Suppl.*, **52**, 399.
Shao, C. Y., and Liller, W. 1972, unpublished.
Shields, G. 1978, *Ap. J.*, **219**, 559.
Shklovsky, I. S. 1956, *Astr. Zh.*, **33**, 222.
Spitzer, L., and Jenkins, E. B. 1975, *Ann. Rev. Astr. Ap.*, **13**, 133.
Stone, R. P. S., and Baldwin, J. A. 1983, *M.N.R.A.S.*, **204**, 347.
Torres-Peimbert, S., and Peimbert, M. 1977, *Rev. Mexicana Astr. Ap.*, **2**, 181 (TPP).
Torres-Peimbert, S., Pena, M., and Daltabuit, E. 1981, in *The Universe at Ultraviolet Wavelengths* ed. R. Chapman (NASA CP-2171), p. 641.
Vedder, P. W., and Clark, G. W. 1982, *Bull. AAS*, **14**, 915.
Webster, B. L. 1969, *M.N.R.A.S.*, **143**, 79.
Weedman, D. W. 1968, *Ap. J.*, **153**, 49.
Wiese, W. L., Smith, M. W., and Glennon, B. M. 1966, NSRDS-NBS-4.
Wilkes, B. J., Ferland, G. J., Hanes, D., and Truran, J. W. 1981, *M.N.R.A.S.*, **197**, 1.
Wood, P. R., Bessell, M. S., and Fox, M. W. 1983, *Ap. J.*, **272**, 99.
Zeippen, C. 1982, *M.N.R.A.S.*, **198**, 111.

M. J. Barlow and R. E. S. Clegg: Department of Physics and Astronomy, University College London, Gower Street, London WC1E 6BT, England

J. P. Harrington: Astronomy Program, University of Maryland, College Park, MD 20742

J. R. Walsh: Anglo-Australian Observatory, P.O. Box 296, Epping, NSW 2121, Australia